Nerve Growth Factor transfer from cardiomyocytes to innervating sympathetic neurons activates TrkA receptors at the neuro-cardiac junction

Lolita Dokshokova [1,2,3*], Mauro Franzoso [1,*], Anna Di Bona [4], Nicola Moro [1], Josè Sanchez-Alonso-Mardones [3], Valentina Prando [1], Michele Sandre [1], Cristina Basso [4], Giuseppe Faggian [2], Hugues Abriel [5], Oriano Marin [1], Julia Gorelik [3], Tania Zaglia [1,#], Marco Mongillo [1,6,#]

This is an Accepted Article that has been peer-reviewed and approved for publication in The Journal of Physiology, but has yet to undergo copy-editing and proof correction. Please cite this article as an 'Accepted Article'; doi: 10.1113/JP282828.

[1], Department of Biomedical Sciences, University of Padova, via Ugo Bassi 58/B, 35121, Padova, Italy;

[2], Division of Cardiac Surgery, University of Verona, Verona, Italy;

[3], National Heart and Lung Institute, London, United Kingdom of Great Britain & Northern Ireland;

[4], Department of Cardiac, Thoracic, Vascular Sciences and Public Health, University of Padova, via Giustiniani 2, 35131, Padova, Italy;

[5], Institute of Biochemistry and Molecular Medicine, University of Bern, Bühlstrasse 28, 3012 Bern, Switzerland;

[6], CNR Institute of Neuroscience, Viale G. Colombo 3, 35121 Padova, Italy.

*, equal contribution

#, co-corresponding authors

Correspondence to:

Marco Mongillo, MD, PhD

Department of Biomedical Sciences, University of Padova, Via Ugo Bassi 58/B, 35121 Padova, Italy

Tel: +39 0497923229

Fax: +39 0497923250

e-mail: marco.mongillo@unipd.it

Tania Zaglia, PhD

Department of Biomedical Sciences, University of Padova, Via Ugo Bassi 58/B, 35121 Padova, Italy

Tel: +39 0497923294

Fax: +39 0497923250

e-mail: tania.zaglia@unipd.it

Running title: 'Cardiomyocyte-to-neuron' communication at neuro-cardiac junctions.

KEY POINT SUMMARY

The integration of *ex vivo* and *in vitro* data, described in this manuscript, together with our previous demonstration that sympathetic neurons (SNs) contact target cardiomyocytes (CMs) at the neuro-cardiac junction (NCJ), which underlies intercellular synaptic communication (Prando *et al.*, 2018), demonstrate that:

- CMs are the cell source of Nerve Growth Factor (NGF), required to sustain innervating cardiac SNs;

- NCJ is the place of the intimate liaison, between SNs and CMs, allowing on the one hand neurons to peremptorily control CM activity, and on the other, CMs to adequately sustain the contacting, everchanging, neuronal actuators;

- alterations in NCJ integrity may compromise the efficiency of 'CM-to-SN' signaling, thus representing a potentially novel mechanism of sympathetic denervation in cardiac diseases.

Keywords:

Cardiac Sympathetic Neurons;

Cardiomyocytes;

Neuro-Cardiac Junction;

Nerve Growth Factor;

NGF receptor.

ABSTRACT

Background: Sympathetic neurons densely innervate the myocardium with non-random topology and establish structured contacts (i.e. neuro-cardiac junctions, NCJ) with cardiomyocytes, allowing synaptic intercellular communication. Establishment of heart innervation is regulated by molecular mediators released by myocardial cells. The mechanisms underlying maintenance of cardiac innervation in the fully developed heart, are, however, less clear. Notably, several cardiac diseases, primarily affecting cardiomyocytes, are associated to sympathetic denervation, supporting that retrograde 'cardiomyocyte-to-sympathetic neuron' communication is essential for heart cellular homeostasis.

Objective: We aimed to determine whether cardiomyocytes provide Nerve Growth Factor (NGF) to sympathetic neurons, and the role of the NCJ in supporting such retrograde neurotrophic signaling.

Methods and Results: Immunofluorescence on murine and human heart slices shows that NGF and its receptor, Tropomyosin-receptor-kinase-A, accumulate respectively in the pre- and post-junctional sides of the NCJ. Confocal immunofluorescence, scanning ion conductance microscopy and molecular analyses, in co-cultures, demonstrate that cardiomyocytes feed NGF to sympathetic neurons, and that such mechanism requires a stable intercellular contact at the NCJ. Consistently, cardiac fibroblasts, devoid of NCJ, are unable to sustain SN viability. ELISA assay and competition binding experiments suggest that this depends on the NCJ being an insulated microenvironment, characterized by high [NGF]. In further support, real-time imaging of Tropomyosin-receptor-kinase-A-vesicle movements demonstrate that efficiency of neurotrophic signaling parallels the maturation of such structured intercellular contacts.

Conclusions: Altogether, our results demonstrate the mechanisms which link sympathetic neuron survival to neurotrophin release by directly innervated cardiomyocytes, conceptualizing sympathetic neurons as *cardiomyocyte-driven* heart drivers.

ABBREVIATIONS AND ACRONYMS

β-AR, β-Adrenoceptors; CM, cardiomyocyte; cSN, cardiac Sympathetic Neuron; cTnI, cardiac Troponin I; GFP, Green Fluorescent Protein; mo., months; HF, Heart Failure; IF, immunofluorescence; MI, Myocardial Infarction; MOI, Multiplicity of Infection; NCJ, Neuro-Cardiac Junction; NE, Noradrenaline; NGF, Nerve Growth Factor; NGF-R, NGF-receptor; NMJ, Neuro-Muscular Junction; SICM, Scanning Ion Conductance Microscopy; SN, Sympathetic Neuron; SNS, Sympathetic Nervous System; TEM; Transmission Electron Microscopy; TH, Tyrosine Hydroxylase; TrkA, Tyrosine Kinase Receptor A.

INTRODUCTION

Sympathetic neurons (SNs) densely innervate the heart of mammals, including humans (Wichter *et al.*, 2000; Kawano *et al.*, 2003) with a well-defined topology, which is finely regulated by the myocardium itself (Ieda *et al.*, 2004; Ieda *et al.*, 2007; Franzoso *et al.*, 2016; Zaglia & Mongillo, 2017). The precise species-specific geometry of myocardial sympathetic innervation is finalized to ensure optimal electrical and contractile performance, and allows continuous adaptation of heart function through acute (i.e. chronotropic, inotropic and lusitropic) and chronic (i.e. regulation of gene expression) effects of neuronal inputs on target cardiomyocytes (CMs) (Shan *et al.*, 2010; Zaglia *et al.*, 2013; Franzoso *et al.*, 2016; Larsen *et al.*, 2016; Prando *et al.*, 2018; Pianca *et al.*, 2019). Dysfunction in the neurogenic control of cardiac activity features in several cardiovascular diseases, including myocardial hypertrophy, ischemia/infarction (MI) and heart failure (HF), all conditions characterized by increased arrhythmic incidence, associated to either enhanced sympathetic drive or reduced SN transmission (Schäfers *et al.*, 1998; Kaye *et al.*, 2000; Miyauchi *et al.*, 2003; Zhou *et al.*, 2004; Hasan *et al.*, 2006; Kimura *et al.*, 2007; Gardner *et al.*, 2016; Herring *et al.*, 2019). While the effects of cardiac hyperinnervation, heightening CM neuronal stimulation, have been subject of intense research, and are now well-defined (Cao *et al.*, 2000*a*, 2000*b*; Miyauchi *et al.*, 2003; Franzoso *et al.*, 2016), the consequence of cardiac SN (cSN) degeneration is only recently being appreciated. On this trail, while cardiac neurons may primarily be affected in several

neurodegenerative disorders (e.g. Parkinson's, Huntington's disease) (Kobal *et al.*, 2004; Orimo *et al.*, 2007; Kiriazis *et al.*, 2012), in other cases, SN degeneration follows CM defect (e.g. familial hypertrophic cardiomyopathies) (Schäfers *et al.*, 1998; Li *et al.*, 2000; Terai *et al.*, 2003). Such observation guided us to investigate the mechanisms of retrograde 'CM-to-SN' communication, and its role in the homeostasis of cardiac sympathetic innervation.

Recently, in line with previous evidence (Scherbakova *et al.*, 2007), we demonstrated that each cSN varicosity contacts target CMs at the Neuro-Cardiac Junction (NCJ), an intercellular contact structure which, in analogy to the well-known Neuro-Muscular Junction (NMJ), allows neurons to interact intimately with CMs, enabling to control cardiac activity with high precision and efficiency (Prando *et al.*, 2018; Pianca *et al.*, 2019). It remains elusive, however, whether such direct 'cell-to-cell' coupling is also involved in reverse CM-to-SN signaling, which would thus identify the NCJ as hub of bi-directional intercellular communication in the heart.

It is well known that CMs synthesize and release neurotrophic and neuro-repellent factors, together tailoring the establishment and topology of the cardiac sympathetic network during development (Lockhart *et al.*, 1997; Glebova & Ginty, 2004; Ieda *et al.*, 2004; Ieda *et al.*, 2007; Habecker *et al.*, 2008; Lorentz *et al.*, 2010; Habecker *et al.*, 2016). In addition, SN viability depends on the continuous neurotrophin supply (mainly NGF in the heart), typically provided by the target organ (Heumann *et al.*, 1984; Shelton & Reichardt, 1984; Lockhart *et al.*, 1997; Zweifel *et al.*, 2005; Habecker *et al.*, 2008; Habecker *et al.*, 2016). Consistently, post-ischemic sympathetic denervation has been attributed to CM damage, affecting neurotrophin-dependent SN sustainment.

Thus, although the general concept that sympathetic innervation is regulated by the cardiac muscle is acknowledged, the detailed physiology of 'CM-to-neuron' neurotrophin exchange has been poorly explored. To address this point, we combined the analysis of murine and human heart with *in vitro* assays in SN/CM co-cultures. The morphology and biophysics of the NCJ were characterized using confocal

microscopy, Scanning Ion Conductance Microscopy (SICM), morphometric analyses, live imaging of NGF-receptor (NGF-R) trafficking, gene silencing and pharmacologic tests. Our results show that CMs directly exchange NGF with the innervating neurons, and that the NCJ is the functional unit where muscle cells nourish contacting neurons, supporting that integrity of the cardiac sympathetic network relays on properly-functioning CM-to-SN communication

METHODS

We declare that all investigators involved in the study understand the ethical principles under which the journal operates and that the work complies with the animal ethics checklist of the journal (Grundy, 2015).

Human heart sample processing and immunofluorescence (IF). We analyzed heart samples from three male subjects (age: 45±8 yrs) died for extra-cardiac causes (accidents), acquired during routine post-mortem clinical investigations, and archived at the Institute of Pathological Anatomy of the University of Padova. Samples were anonymous to the investigators and used in accordance with the "Recommendation (CM/Rec(2016)6) of the Committee of Ministers to member States on research on biological materials of human origin", released by the Council of Europe, as received by the Italian National Council of Bioethics. Samples were analysed using protocols previously described in (Zaglia *et al.*, 2016). The primary and secondary antibodies, and chemicals, used in this study are listed in **Tables 1-3**.

Ethical Approval. All experimental procedures in murine models were approved by the Ministry of Health (Ufficio VI), in compliance with the Animal Welfare Legislation (VIMM C-53 and C-54). All procedures were performed by personnel with documented formal training and previous experience in experimental animal handling and care. All procedures were refined prior to initiating the study, and the number of animals was calculated to use the least number needed to achieve statistical significance, according to sample power calculations.

Origin and Source of Animals. In this study, we used P1-P3 and adult (3 mo.) Sprague-Dawley male rats (Harlan, Milan, Italy). Animals were maintained in individually ventilated cages in an Authorized Animal Facility (authorization number 175/2002A) under a 12:12 hours light/dark cycle at a controlled temperature and had access to water and food available *ad libitum.* Rats were killed by cervical dislocation (in accordance with Annex IV of European Directive 2010/63/EU). In adult rats, sedation with 3% isofluorane (v:v in O2) was performed before cervical dislocation.

IF analysis of rodent hearts. Hearts were harvested from adult rats, fixed in 1% paraformaldehyde (PFA) (w:v in PBS; Sigma Aldrich), and processed as described in (Zaglia *et al.*, 2013). Ten µm thick cryosections were obtained using a cryostat (Leica 1860) and processed for IF, as previously described (Zaglia *et al.*, 2013). The primary and secondary antibodies, as well as chemicals used in this study are listed in **Tables 1-3**.

Analysis of SNAP25 and NGF distribution at the neuro-cardiac contacts. Analysis was performed on confocal z-series images post-processed using ImageJ (Wayne Rasband, Bethesda, MD, USA). Three dimensional images were rendered and fluorescence intensity and displacement were measured along parallel lines manually drawn in correspondence of, or away from, the NCJ, identified by morphology.

Establishment of Sympathetic Neuron/Cardiomyocyte co-cultures. Co-cultures between SNs isolated form the superior cervical and stellate ganglia, and CMs from P1-P3 neonatal rat, were set up as described in (Prando *et al.*, 2018; Pianca *et al.*, 2019). We here analyzed 2, 4, 7, 10, and 14 days co-cultures. In a subset of experiments (i.e. assessment of TrkA movements), co-cultures were established between rat neonatal CMs (P1-P3) and PC12-derived SNs, as described in (Prando *et al.*, 2018).

Establishment of Sympathetic Neuron/Cardiac Fibroblasts (CFs) co-cultures. CFs were obtained by plastic adhesion-based separation during CM preparation. Cells were expanded, seeded in laminin-coated coverslips at a density of 100 cells/mm^2. The SN:CF ratio was 1:25. Cells were maintained in the same culture conditions and analyzed at the same time points as SN/CM cultures (see above).

Scanning Ion Conductance Microscopy (SICM). SICM is a contactless imaging method in which the surface of a cellular sample is scanned by an electrolyte solution-loaded nanopipette, continuously measuring the resistance established between the cell and pipette, which depends on their reciprocal distance (Hansma *et al.*, 1989). All topographical images were recorded using the SICM hopping mode (Novak *et al.*, 2009). The tip size of the nanopipette was ~100nm (80-100MΩ), pulled from a borosilicate glass capillary (IntraCel BF100-50-7.5) with a laser puller (ItraCel, Sutter Instrument Co, P-2000). Cells were bathed in "extracellular" solution, while the pipette was filled with "intracellular" solution. The pipette manipulator operates vertical movements along the Z direction, towards the cell surface, and by recording the pipette coordinates when a predetermined current resistance is detected, a topographic map of the scanned surface can be obtained using the software routine SICMView. The three dimensional topological characteristics of the scanned object, such as Volume, Surface area, Surface contact and Height were calculated by SICM Image viewer (Novak *et al.*, 2009).

***In vitro* IF analysis.** Cells were fixed with 3.7% formaldehyde (Sigma) at 4°C for 30 min., permeabilized with 0.1% Triton (v:v in PBS) (Sigma Aldrich) for 5 min. and incubated with the appropriate primary antibody for 2 hours at 37°C. The primary and secondary antibodies, and chemicals, used in this study are listed in **Tables 1-3**.

Evaluation of SN varicosity morphometry. To analyse the size of varicosities, ROIs were manually drawn on TH-positive enlargements along neuronal processes and quantitated on the maximal projection image obtained from a 10-image series along the Z-axis and rendered using ImageJ. Enlargements were defined as axonal segments larger than twice as much the average axonal thickness in the same sample. Inter-varicosity distance was then measured with *Image J*, by calculating the distance along a line manually drawn between subsequent varicosities.

***In vitro* Transmission Electron Microscopy (TEM) analysis.** TEM analysis was performed in SN/CM co-cultures, following the protocol described in (Prando *et al.*, 2018).

Imaging of TrkA-DsRed2 vesicle movements in co-cultures. SN/CM co-cultures were established as described above. SNs were infected with an adenoviral vector encoding TrkA-DsRed2 (Vector BioLabs) at a Multiplicity of Infection (MOI) of 35. After 24 hours, the virus was removed, and the medium freshly replaced, and imaging was performed at 48 hours from infection. In detail, we compared TrkA dynamics in 4 (early) *vs.* 14 (mature) day co-cultures. During imaging experiments, cells were maintained in Tyrode solution (125 NaCl, 5 KCl, 1 Na_3PO_4, 1 $MgSO_4$, 5.5 glucose, 1.8 $CaCl_2$, 20 HEPES, in mM/L, pH 7.4). Cells were analysed in a culture dish incubator, at controlled temperature (37°C), atmosphere and pH. TrkA-DsRed2 vesicle movements were recorded by acquiring images every 30s with a confocal microscope (Leica SP5), equipped with an oil immersion 1,3NA, 63X objective. Kymographs of the time-lapse images were obtained with the ImageJ® plugin *kymograph*, as described in (Jakobs *et al.*, 2019).

Cultured cardiomyocyte transfection. Cultured CMs were transfected using transfectin (Bio Rad), following the manufacturer' instructions. Cells were co-transfected with a plasmid encoding Green Fluorescent Protein (GFP) and small hairpin RNAs, including: shRNA NGF mRNA (encoding for the 2 transcript variants of the β polypeptide (XM_003749364.1, XM_227525.6) (Sigma-Aldrich)); SIC001 (Sigma-Aldrich) as control.

RTqPCR analysis. The analysis was performed following the protocol described in (Zaglia *et al.*, 2014). The oligoes used in this study are listed in **Table 4**.

Western blotting. This procedure was performed as described in (Zaglia *et al.*, 2014).

ELISA assay. To estimate NGF concentration in the CM conditioned medium, we used the ChemiKine NGF sandwich ELISA Kit (Chemicon), following the manufacturer's instructions.

Statistical analysis. Statistical analysis was performed using GraphPad Prism 8. Normality of data distribution was assessed with Shapiro-Wilk test. Unpaired t-test (for 2 groups) or One-Way ANOVA, with Brown-Forsythe and Welch corrections (for 3 or more groups) were used for normally distributed data.

Non-parametric Mann-unpaired t-test (for 2 groups) or One-Way ANOVA (for 3 or more groups) were used for normally distributed data with equal variance. Unpaired t-test with Welch's correction (for 2 groups) or Brown-Forsythe and Welch ANOVA (for 3 or more groups) were used for normally distributed data with unequal variance. Mann-Whitney test (for 2 groups) or Kruskal-Wallis test (for 3 or more groups) were used for non-normally distributed data. Data distribution is represented by individual values, with mean and error bars representing 95% confidence interval. A P value <0.05 was considered statistically significant.

RESULTS

1. In mammalian hearts, the neurotrophin-signaling elements preferentially accumulate at the neuro-cardiac interface

We have shown that, in mammalian hearts, structured interaction between catecholamine-releasing neuronal varicosities and CM membrane (i.e. NCJ) underpins localized and cell-directed *anterograde* neuro-cardiac communication (Prando *et al.*, 2018). Here, we tested the hypothesis that *retrograde* 'CM-to-SN' neurotrophic signaling could also take place electively at the NCJ.

Confocal IF in ventricular cryosections of mammalian hearts showed that the vast majority of neuronal processes are sympathetic, and as such, markers of neuro-exocytosis (e.g. SNAP25) were used as *bona fide* indicators of cSNs (Prando *et al.*, 2018). Co-IF in rat heart sections demonstrated that SNAP25 positive neuronal processes also express the high-affinity NGF receptor, TrkA, which was found in the enlargements identifiable as varicosities (**Fig.1A**). Staining of the sections with an anti-NGF antibody showed immunoreactive vesicles in CMs, which clustered in a roughly 2μm deep submembrane space, and appeared to mirror the position of the pre-synaptic neuronal varicosities, in the majority (>60%) of neuro-cardiac interfaces analysed (**Fig.1B**). Consistently, sub-microscopic analysis of the immunostained sections revealed high intensity NGF puncta (in green) spread in the CM cytosol, accompanied by neurotrophin clusters aligned along the portion of the CM membrane directly contacted by the SN (**Fig.1C**). This was in line with the results of morphometric image analysis aimed to trace pre-synaptic

SNAP-25 and post-synaptic NGF distribution, showing that the highest NGF fluorescence intensity, in the CM, corresponded to the peak of SNAP-25 signal on the neuron (**Fig.1D**). In addition, NGF was detected along the neuronal process, suggesting that CM-released neurotrophin could be sensed and locally internalized, *via* TrkA, by the contacting SN (**Fig.1B**). Interestingly, the presence of NGF in CM-innervating neuronal processes and the preferential localization of the neurotrophin in the CM submembrane space, at neuro-cardiac contacts, were detected, and confirmed by morphometric analysis, in myocardial samples from post-mortem human hearts, proving the principle that the aspects described above hold true in the normal human heart (**Fig.2A-C**).

Thus, the arrangement of NGF vesicles in CMs and of NGF-sensing receptors on SNs, suggests that exchange of neurotrophin between the two cell types may take place locally, and that the NCJ may thus be poised to sustain retrograde (myocyte-to-neuron) neurotrophic signaling.

2. The neuro-cardiac junction matures in time while neurons become independent from exogenous NGF

To investigate retrograde neurotrophin-mediated communication at the single cell level, we used a previously validated *in vitro* system, based on co-cultures between SNs and CMs (Prando *et al.*, 2018; Pianca *et al.*, 2019). Our data confirmed the common recognition (Mains & Patterson, 1973; Greene, 1977) that SNs, cultured *in vitro*, require addition of NGF to the medium for survival and maturation (**Fig.3A-B**). In fact, absence of NGF in the culture medium only allowed a negligible and unquantifiable amount of neurons to be detected in culture after 7 days. Remarkably, we soon noted, however, that when SNs were co-cultured with CMs, they developed normally, irrespective of exogenous NGF (**Fig.3C-E**). We excluded this to result from the presence of NGF in the serum, as our co-culture medium was serum-free.

Based on our previous results (Prando *et al.*, 2018), we compared (early) 7 *vs.* (mature) 14 day co-cultures and, notably, we did not observe differences in SN density (number of cell soma/area (mm^2), 7 days, +NGF:17.05±7.60 *vs.* -NGF:14.99 ±11.61; 14 days, +NGF:10.42±7.80 *vs.* 14 days, -NGF:9.39±3.29, data expressed as mean±SD; p=ns) and in the morphology of neuronal processes (i.e.

size of varicosities and interindividual distance between varicosities), in the presence *vs.* absence of NGF in the culture medium, at either time point (**Fig.3C-E**).

Moreover, morphometric analyses demonstrated that SN varicosities grew in time (area of Tyrosine Hydroxylase (TH)+ enlargements) to a similar extent in the absence or the presence of exogenous NGF (**Fig.3D**). The only difference, which was evident already at qualitative level, in the two conditions was the increased neuronal axonal sprouting, in NGF-added co-cultures (**Fig.3C**), consistent with the effect of diffuse stimulation of neurons with NGF in the medium. These results suggest that CMs represent the cell source of neurotrophin, required to sustain neurons. In further support, quantitation of NGF in protein extracts from CMs, maintained in culture for up to 14 days, demonstrated that cell maturation is accompanied by opposite changes in the relative content of pro-NGF *vs.* mature NGF forms, the latter significantly increasing with time (**Fig.4A**). Such results, suggesting progressive maturation of post-transcriptional processing of the neurotrophin, support the time-dependency of SN maturation elicited by targeted CMs. In addition, they are in line with the findings in postnatal heart development, which show progressive increase in cardiac content of mature NGF between partially innervated neonatal *vs.* fully innervated adult hearts (**Fig.4B**). Notably, confocal IF demonstrated that NGF was detectable in CMs in both early and mature co-cultures, with a vesicular distribution around the cell nucleus, consistent with the production and maturation sites of the neurotrophin, and tended to accumulate underneath the CM membrane portion contacted by the neuronal process (**Fig.4C-D**).

We subsequently sought to determine whether target-derived neurotrophic effects depended solely on NGF availability or if they required cell-specific structured interactions. We thus compared neuronal morphology and NGF uptake in co-cultures set up between SNs and either CMs or cardiac fibroblasts (CFs), the latter previously shown (Mias *et al.*, 2013), and confirmed by us, to synthetize high amount of mature NGF (**Fig.5A**). Interestingly, in 14-days co-cultures, the mean NGF immunoreactivity in the portion of SN processes contacting CFs (**Fig.5B**) was lower than that measured in SN processes innervating CMs (**Fig.5C**). This result suggests that, despite CFs have high availability of NGF, efficiency of its uptake by

SNs is reduced. In line with this, in SN/CF co-cultures, removal of NGF caused a significant decrease in neuronal density (more than 50±4% in 7 days cultures; more than 80±7% in 14 days cultures), accompanied by a reduction in the size of neuronal varicosities, when compared to those from SNs contacting CMs, in the same culture conditions (**Fig.5D-E**).

To further isolate the macroscopic effect of prolonged cell-to-cell interaction on the maturation of intercellular contact sites, we took advantage from our previous demonstration that, contrary to CMs, CFs are unable to establish stable and structured interaction with innervating SNs (Pianca *et al.*, 2019). We thus assessed the topography of SN varicosities, in SN/CM and SN/CF co-cultures, in the three-dimensions (3-D), using Scanning Ion Conductance Microscopy (SICM). SICM allows to quantitate at high resolution the surface area and volume of the neuronal varicosity in contact with the target cell (CM or CF). Coordinates of the single voxel of the scanned surface (i.e. x,y,z) are assigned to a 3-D matrix, rendered as image with a specific analysis software. The output which can be extrapolated includes the crude morphology of the scanned object (e.g. varicosity), the direct measure of the object height, its surface area and calculated volume. In this study, we firstly focussed on SN/CM co-cultures, at different time points (i.e. 2, 4,10 and 14 days), maintained in the absence of NGF. From the morphologic point of view, the initial (@ 2 days) tubular shape of neuronal processes developed, from 4 days onwards, enlargements of progressively higher surface area and volume, which stand out from the CM layer (height), achieving the typical pearl-necklace morphology of SNs (**Fig.6A-B**). As shown previously (Prando *et al.*, 2018) growth of varicosities was maximal at 14 days in culture (**Fig.6C**), while no further changes occurred with more prolonged time in culture. Remarkably, the trophic effect of CMs on contacting varicosities was independent from the presence of NGF in the culture medium, as no differences in morphology and size were observed with or without the neurotrophin in the culture medium (**Fig.6D**).

On the contrary, the varicosity size of neuronal processes contacting CFs did not increase in time and, after the same period in culture, all morphometric parameters remained significantly lower than those calculated in neurons innervating CMs (**Fig.6E**).

Altogether, this data suggests that CMs may be a source of neurotrophin for the innervating neurons, and strongly supports that retrograde 'target cell-to-SN' neurotrophic signaling requires the establishment of structured and stable intercellular contact sites (i.e. NCJs).

3. Cardiomyocyte-derived NGF is essential to sustain the innervating sympathetic neurons

If CM-released NGF were necessary to sustain innervating SNs, we would expect interference with its production by CMs to result in degeneration of the innervating neurons. We thus transfected CMs with plasmids encoding for either siRNA for NGF (si44), designed to ablate NGF expression, or a scramble plasmid, as control. A GFP-encoding plasmid was combined with each siRNA to identify successfully transfected CMs (**Fig.7**). Our results show that si44 caused a (61.05±5.85%) decrease in NGF expression, compared to controls, and did not interfere with the expression of others CM neurotrophins, such as NT3 (**Fig.7A**). In addition, cell transfection did not affect CM viability and morphology, since no significant differences in sarcomere organization (**Fig.7B**), CM area or density were observed (cell area, un-transfected CMs: 958±284 *vs.* scramble CMs: 1176±462 *vs*. NGF siRNA CMs: 1117±592, in μm^2, data expressed as mean±SD; p=ns) (cell density, un-transfected CMs: 394±115 *vs.* scramble CMs: 410±76 *vs.* NGF siRNA: 341±95, in cells/mm^2, data are expressed in as mean±SD; p=ns). Consistent with our hypothesis, SN innervating NGF-silenced CMs appeared fragmented and had smaller TH-marked varicosities, compared to controls (**Fig.7C-D**). Notably, all these effects were prevented by NGF addition to the culture medium.

These results prove that SN trophism depends on NGF directly provided by the innervated CMs.

4. Maturation of intercellular 'sympathetic neuron-cardiomyocyte' contacts parallels TrkA directional signaling

It is well-accepted that NGF plays its role in sustaining SN development, growth and survival, through activation of the high affinity neurotrophin receptor, TrkA (Chao, 2003; Zweifel *et al.*, 2005; Reichardt,

2006). Consistently, confocal IF showed that SNs expressed, in both early (4 days) and long (14 days) term co-cultures, the NGF-receptor TrkA (**Fig.8A**). This evidence, together with the preferential accumulation of NGF underneath the portion of CM membrane contacted by the neuronal process (**Fig.4C-D**), suggest that the co-cultures replicate well the features observed in the intact myocardium, and are thus suited to interrogate the mechanisms of intercellular neurotrophin signaling, *in vitro*. Moreover, based on the data acquired thus far, we expect that activation of neuronal TrkA initiates at the neuro-cardiac interface and that the efficiency of intercellular signaling increases with NCJ maturation.

To quantitate activation of NGF/TrkA signaling in co-cultures, we infected SNs with a construct encoding the fluorescent fusion protein, TrkA-DsRed, and used confocal time-lapse imaging to monitor TrkA trafficking, as an effect of receptor activation by NGF (**Fig.8B**). We thus compared neuronal TrkA-DsRed2 movements in early *vs.* mature SN/CM co-cultures, which were quantified through kymograph analysis (**Fig.8C**). Consistent with the literature (Zweifel *et al.*, 2005), both stationary and bi-directional (i.e. anterograde and retrograde) moving red fluorescent vesicles were detected in SN processes. While in early co-cultures the relative fractions of anterograde and retrograde movements of TrkA dots were comparable, and higher than that of stationary dots, we observed a significant increase in the percentage of directionally moving and stationary TrkA dots in mature co-cultures (**Fig.8D**). These results indicate increased NGF/TrkA signalling from the distal portions of the neuron to the soma, which may depend on higher NGF availability in target cells and maturation of the NCJ allowing more efficient intercellular communication (see **Figs.4** and **6**). In line with the reduced neurotrophic effects of CFs, which lack structured NCJs (see above), on innervating neurons, directional TrkA trafficking was reduced by more than 70% in SN/CF co-cultures (retrograde movements, on CMs: 52.61±31.93 (n=41) *vs.* on CFs: 12.90±11.66 (n=20); $p<0.0001$).

5. The Neuro-Cardiac Junction defines a high [NGF] extracellular signaling domain

The results collected thus far prompted us to investigate the biophysical mechanism underscoring CM-SN signaling, and we considered two hypotheses: i) CMs sustain neuronal viability and trophism by

releasing diffusely high amounts of NGF or ii) CMs feed neurons selectively at the single contact site with SN varicosities by releasing NGF in a targeted and efficient way at the NCJ. To verify whether CMs were able to release enough NGF in the medium to sustain SN viability, we collected the medium conditioned by CMs and used it in a pure SN culture. Interestingly, CM-conditioned medium caused a (55±3%) reduction in neuronal density, which was comparable to the effect of NGF deprivation on SNs alone. In agreement with this result, [NGF] in the CM-conditioned medium was about 1000-fold lower (1.61±1, in pg/ml) than the minimal concentration required for neuronal survival. These results exclude that the bulk NGF amount released by CMs is sufficient to sustain SNs, and surmise a model whereby elevated [NGF], activating TrkA signaling, is locally achieved at the SN/CM contact site. This hypothesis is in line with our previous demonstration that the NCJ outlines a diffusion-restricted signaling domain (Prando *et al.*, 2018), characterized by specific protein enrichment and reduced cell-to-cell intermembrane distance (**Fig.9A**).

To test whether intercellular NGF signaling occurred predominantly at the NCJ, we set up a NGF inhibition assay by using either: i) an anti-NGF antibody or ii) the membrane permeable TrkA antagonist, k252a (Berg *et al.*, 1992) (**Fig.9B**). We initially tested both molecules in cultures of SNs alone, to determine the concentration which caused a significant decrease of neuronal viability, in the presence of 8nM NGF in the culture medium (**Fig.9C**). Subsequently, we treated mature co-cultures, deprived of exogenous NGF, with the same molecules (i.e. anti-NGF, k252a) at the same concentration, and notably, while k252a substantially replicated the effect on pure SN cultures, the anti-NGF antibody had negligible effects on SN viability (**Fig.9D**). Given the physical-chemical differences between the two compounds, and the significant steric hindrance of the anti-NGF antibody, this result suggests that the barriered CM-SN contact site opposes to the permeation of the antibody in the intercellular space.

To infer the NGF concentration active in the NCJ, we compared the effect of k252a on neuronal viability in co-cultures (in which NGF was only derived from CMs), with that of k252a on pure SN cultures treated with increasing [NGF] in the culture medium. The results of such estimate suggest that the NGF concentration active at the contact site is in the order of 1.4±0.03nM (**Fig.9E**).

Taken together, these results suggest that the NCJ is an isolated microenvironment protected from diffusion and characterized by high NGF concentrations.

DISCUSSION

This study investigates the mechanisms of neurotrophic communication between cardiac cells and heart-innervating SNs. Our results indicate that CMs provide vital support to neurons through direct exchange of NGF, which takes place locally at the neuro-cardiac interaction site. We showed that as CMs establish structured intercellular contacts, stable in time, with neurons, they guarantee more efficient neurotrophic input than CFs, throughout postnatal development. We thus refine the notion that the target organ sustains its own sympathetic innervation, by identifying the specific cell population responsible for such effect, in physiology. Our data infers that alteration in the NCJ or in NGF signaling, resulting from primary CM injury, may thus underlay heart dysinnervation and clinically relevant cardiac dys-autonomia.

In conventional neuro-cardiology, the Sympathetic Nervous System (SNS) is regarded as the extrinsic modulator of cardiac activity in stress conditions (Zaglia & Mongillo, 2017; Scalco *et al.*, 2021). However, recent biotechnological advancement, which allowed to partially unmask the tangles of cardiac sympathetic innervation, together with the rediscovered curiosity in the physiological mechanisms of neurogenic heart regulation, led to uncovering unexpected roles of cardiac SNS, beyond ignition of the fight-or-flight reaction (for a review see Scalco *et al.*, 2021). An aspect which has only recently been appreciated, is that the mammalian heart is more densely innervated, by SNs, than expected: as example, each CM is simultaneously embraced by several neuronal processes (from 3 to 6), which may originate from sprouted axons of the same or different neurons (Di Bona *et al.*, 2020; Scalco *et al.*, 2021). Furthermore, neurons distribute with a non-random, species-specific topology, which reflects the respective cardiac electrical and mechanical properties (Pianca *et al.*, 2019). The network architecture, established in embryonic or early postnatal development, is designed by molecular mediators released by myocardial cells, either recruiting (i.e. neurotrophic factors, such as NGF) or blocking (i.e. chemorepellent agents, such as semaphorine-3a) axonal growth in a given myocardial territory (Ieda *et al.*, 20074; Ieda *et al.*, 2007; Lorentz *et al.*, 2010; Kimura *et al.*, 2012; Franzoso *et al.*, 2016). Additionally, we and others showed that cSN inputs continue to shape the morphologic and electrophysiologic properties of the adult myocardium, implying that the pattern of cardiac innervation needs to remain unchanged for physiologic cardiac function (Ieda *et al.*, 2007; Franzoso *et al.*, 2016; Habecker *et al.*, 2016; Zaglia & Mongillo, 2017; Pianca *et al.*, 2019; Di Bona *et al.*, 2020). Consistently, like other organs innervated by SNs, the myocardium synthetizes neurotrophins for the entire lifespan, and it is thus fundamental to understand how heart cells deliver neurotrophic signals to SNs (Habecker *et al.*, 2008; Franzoso *et al.*, 2016; Habecker *et al.*, 2016). Cardiac homeostasis is thus based on finely regulated bi-directional communication between neurons and CMs, mutually necessary to ensure cell viability in one direction, and regulation on the other side.

While the effects of anterograde communication between neurons and CMs has been subject of several studies in the last decades, the interest on the retrograde 'CM-to-SN' communication axis has only recently emerged. Research on this topic has been fueled by the

evidence that several diseases, primarily targeting CMs (such as MI and HF), lead to secondary myocardial denervation (Boogers *et al.*, 2010; Kimura *et al.*, 2010; Nishisato *et al.*, 2010; Gardner *et al.*, 2016; Himura *et al.*, 1993; Tapa *et al.*, 2020). Such pathogenetic link has been attributed to failure of neurotrophic signaling from heart to neurons (Habecker *et al.*, 2008; Lorentz *et al.*, 2010; Habecker *et al.*, 2016), but the underlying mechanisms, in both physiology and pathology, are still unclear. A basic unresolved question regards the dynamics of CM neurotrophin input to SNs, and the way it occurs. In other words, do CMs feed neurons organ-wide (implying NGF diffusion in the myocardial interstitium), or through direct hetero-cellular coupling (implying 'simil-synaptic' communication)?

Recently, we and others demonstrated that SNs communicate to target CMs in a synaptic fashion, by releasing NE in a diffusion-restricted intercellular domain (i.e. NCJ), allowing to reach high [NE] at the expense of few neurotransmitter vesicles (Shcherbakova *et al.*, 2007; Prando *et al.*, 2018). In the current study, we extend such discovery to the reciprocal signaling axis, demonstrating that the NCJ is also the election site of CM-dependent neuronal feeding with NGF (Fig.10). In line with this, our confocal IF in heart slices and SN/CM co-cultures adds new pieces to the growing puzzle of molecules concentrating in correspondence of the SN/CM contact site, notably including NGF on the CM side, and its receptor TrkA, on the neuronal one. The evidence that NGF is secreted preferentially at the NCJ suggests that scaffold proteins previously shown to accumulate at the post-synaptic membrane (e.g. cadherins, β-catenin, SAP97) may also play a role in intracellular routing of the neurotrophin (Shcherbakova *et al.*, 2007; Prando *et al.*, 2018). In addition, our results strongly support that the NCJ outlines a low volume/high [NGF] intercellular domain, allowing efficient activation of TrkA signaling, potentially at the expense of few molecules of NGF. In further support of this, the amount of CM-derived NGF is insufficient to prevent cSN death, when added diffusely to the culture medium. Moreover, CFs despite synthetizing high amounts of NGF, fail to sustain SN viability and development in co-culture, likely due to their incapacity to establishing a stable intercellular contact, and as such to direct NGF to innervating neurons. Such central role of the NCJ in 'CM-to-SN 'signaling is highlighted by the demonstration that CM-contacting SNs grew and developed indistinguishable (in term of varicosity size and distance between varicosities) from neurons supplied with high amount of NGF in the medium. In the view of these results, we thus surmise that local communication underlays CM to SN neurotrophin signaling, opening to further mechanistic speculations on the role of the NCJ in both physiology and pathology.

Firstly, one may speculate that the amount of NGF captured by a single varicosity is not sufficient to sustain viability of a complex post-mitotic cell, like a cSN, whose cell body is located in a ganglion distant (i.e. at the level of the neck) from the innervated myocardium (Scalco *et al.*, 2021). However, when considering that i) each single varicosity locally takes up NGF from the innervated CM and ii) each neuronal process is made by numerous regularly distributed varicosities, innervating multiple CMs (Zaglia & Mongillo, 2017; Pianca *et al.*, 2019), we can conjecture that the total amount of NGF reaching the neuronal soma reflects the

summed contribution of innumerable varicosities. This may be thought of as a mechanism to distribute NGF supply among the different providers, protecting neurons from neurotrophin depletion subsequent to regional dysfunction of NGF-making cells. In addition, the most linear inference is that the local nature of NGF input, at specific varicosities, would be lost once TrkA reaches the nucleus. However, the evidence that while retrogradely transported NGF/TrkA exerts effects on neuronal survival and growth, stationary NGF/TrkA signalosomes operate within the single varicosity (Kuruvilla *et al.*, 2000; Zweifel *et al.*, 2005), prompts a mixed model whereby local neurotrophic inputs may activate both local and global cellular effects.

Secondly, although regulation of NGF transcription was not in the scopes of the current research, the evidence that the NCJ is critical for both adrenergic and neurotrophin communication suggests that the two signaling axes may be cross-regulated. This speculation is based on previously published reports showing that catecholamines influence the biosynthesis of NGF, in different cell types, including CMs (Furukawa *et al.*, 1986, 1987, 1989; Kaechi *et al.*, 1993; Hanaoka *et al.*, 1994; Colangelo *et al.*, 1998). Such reciprocal interplay between CM and SNs, and the possibility that SNs might influence NGF synthesis in end organs, has been proposed few years ago (Furukawa *et al.*, 1986), but not pursued further, to the best of our knowledge. If this model held true, it would imply a double-strand bond between CMs and innervating SNs, which realizes in the premises of the NCJ.

Such bidirectional crosstalk between SN activity, CM function and neuronal viability, may impact on common cardiovascular therapies, and in particular the widespread use of β-AR blockers, a cornerstone drug against myocardial remodeling and arrhythmias. On the one hand, whether prolonged treatment with anti-adrenergics chronically impinged on the reciprocal CM/SN axis, it would potentially affect CM sustainment of SN viability, and thus cardiac innervation patterning. This effect could potentially reflect on heterogenous/dysfunctional heart innervation, a condition which has, *per se*, been linked to increased arrhythmic vulnerability. Additionally, primary disruption of the NCJ, arising indirectly from other injury mechanisms (e.g. CM remodeling, myocardial ischemia) could have devastating outcomes, as it would compromise simultaneously both neurogenic heart control and SN viability, which would worsen one another in a vicious cycle. Preservation of a healthy NCJ could therefore represent a novel therapeutic

goal to be sought after in common cardiovascular disorders, including arrhythmogenic syndromes, myocardial infarction and HF.

To conclude, the demonstration that SNs survival is strictly dependent on the directly innervated CM (**Fig.10**) leads to reformulate the concept of sympathetic neurons as “heart drivers” into that of neurons as “CM-driven heart drivers”.

LIMITATIONS OF THE WORK

The authors are aware that there are limitations in this study, which could be addressed in future research, and benefit from further optimization of the *in vitro* model and methods to dynamically investigate neuro-cardiac connectivity and intercellular signaling. Firstly, In the current study, we used a mixed co-culture system, in which neurons and cardiomyocyte development was not restrained by pre-defined patterns of cell seeding. While the use of microfluidic platforms would allow to simplify image quantitation, especially with regards to fluorescent particle tracking, intercellular junction-independent neurotrophin and chemorepellent gradients may form in the culture, thus adding a potentially bias in result interpretation. Secondly, we acknowledge that images in human heart post-mortem tissue is hardly quantifiable and comparable to murine hearts. Given the legal constraints in using human tissue, the tissue is inevitably harder to analyze, and it did in fact require a dedicated protocol. The human data, however, confirm as important proof-of-principle, that the purported concepts are shared among rodent and human hearts.

AUTHOR CONTRIBUTION

L.D. and **M.F.** set up *in vitro* and *ex vivo* methodologies, performed *ex vivo* and *in vitro* experiments, analyzed data, interpreted results and contributed to manuscript preparation; **A.D.B.** performed IF on human heart slices, morphometric and biochemical analyses on heart samples; **N.M.** performed biochemical analyses on CF cell cultures, statistical analysis, and contributed to figure preparation; **J.S.A.** performed SICM experiments and analyses and discussed data; **V.P.** contributed to a subset of *in vitro* experiments, PC12 cell culture and TrkA imaging; **M.S.** analyzed the structure of the compounds used in *in vitro* studies; **C.B.** provided human heart samples; **G.F.** critically discussed data; **H.A.** shared reagents and critically discussed data; **O.M**. analyzed the structure of the compounds used in *in vitro* studies; **J.G.** supervised SICM experiments and critically discussed data; **T.Z.** and **M.M.** designed and supervised the study, interpreted and discuss results and wrote the manuscript.

AKNOWLEDGEMENTS

We are grateful to Dr. Nicola Pianca for technical assistance, and Drs. Raffaele Lopreiato, Giulietta Di Benedetto and Tullio Pozzan for critical discussion.

FUNDING

This work was supported by the University of Padova (StarsWiC2017 “miniheartwork” to M.M.), STARS-SKoOP (UNIPD) to T.Z., and the British Heart Foundation (grant RG/17/13/33173) to J.G. and J.S.A.

DISCLOSURES

Nothing to declare.

ADDITIONAL INFORMATION

Data availability statement

The data that support the findings of this study are available from the corresponding author upon reasonable request.

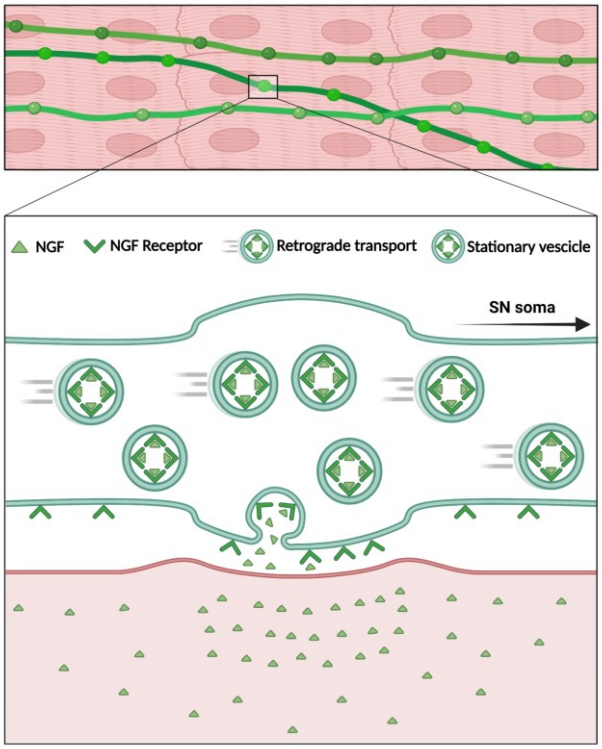

The Journal of Physiology

Abstract figure. Sympathetic neuron (SN, green) varicosities establish synaptic contacts with target cardiomyocytes (CMs, pink), which we previously called Neuro-Cardiac Junction (NCJ, Prando et al. J Physiol 2018). At NCJs, CMs release selectively NGF, which by activating TrkA signaling, is key to sustain neuronal survival.

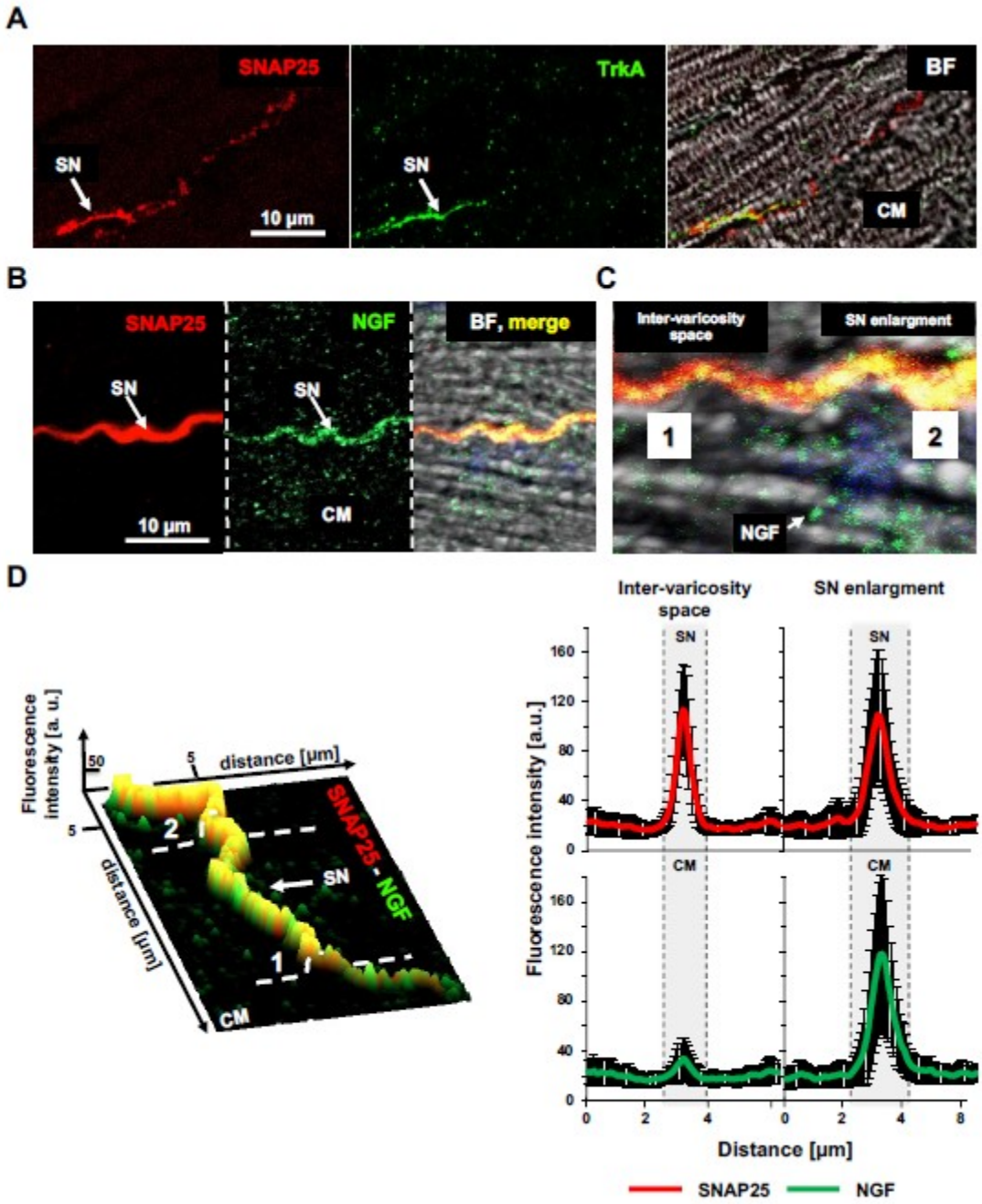

Figure 1. The molecular players of NGF signaling predominantly localize at the Neuro-Cardiac Junction, in rat hearts.

(**A**) Confocal IF analysis of heart sections from adult rats, co-stained with antibodies against SNAP25 (left panel) and TrkA (middle panel). The right panel shows the bright field images (BF). SN, sympathetic neuron; CM, cardiomyocyte. The white arrow indicates the neuronal process. (**B**) Confocal IF analysis of adult rat heart sections, co-stained with antibodies against SNAP25 (left panel) and NGF (middle panel). The right panel shows merged fluorescence and bright field images. The white arrow indicates the SN process. (**C**) Magnified image of panel B. (**D**) Surface rendering of the z-section series of the IF images shown in (**B**) and relative quantification of the fluorescence intensity of SNAP25 (red signal) and NGF (green signal) in correspondence of the neuronal varicosity (2) or the inter-varicosity space (1). Bars represent SD (n=66 neuro-cardiac contacts from 3 different rat hearts).

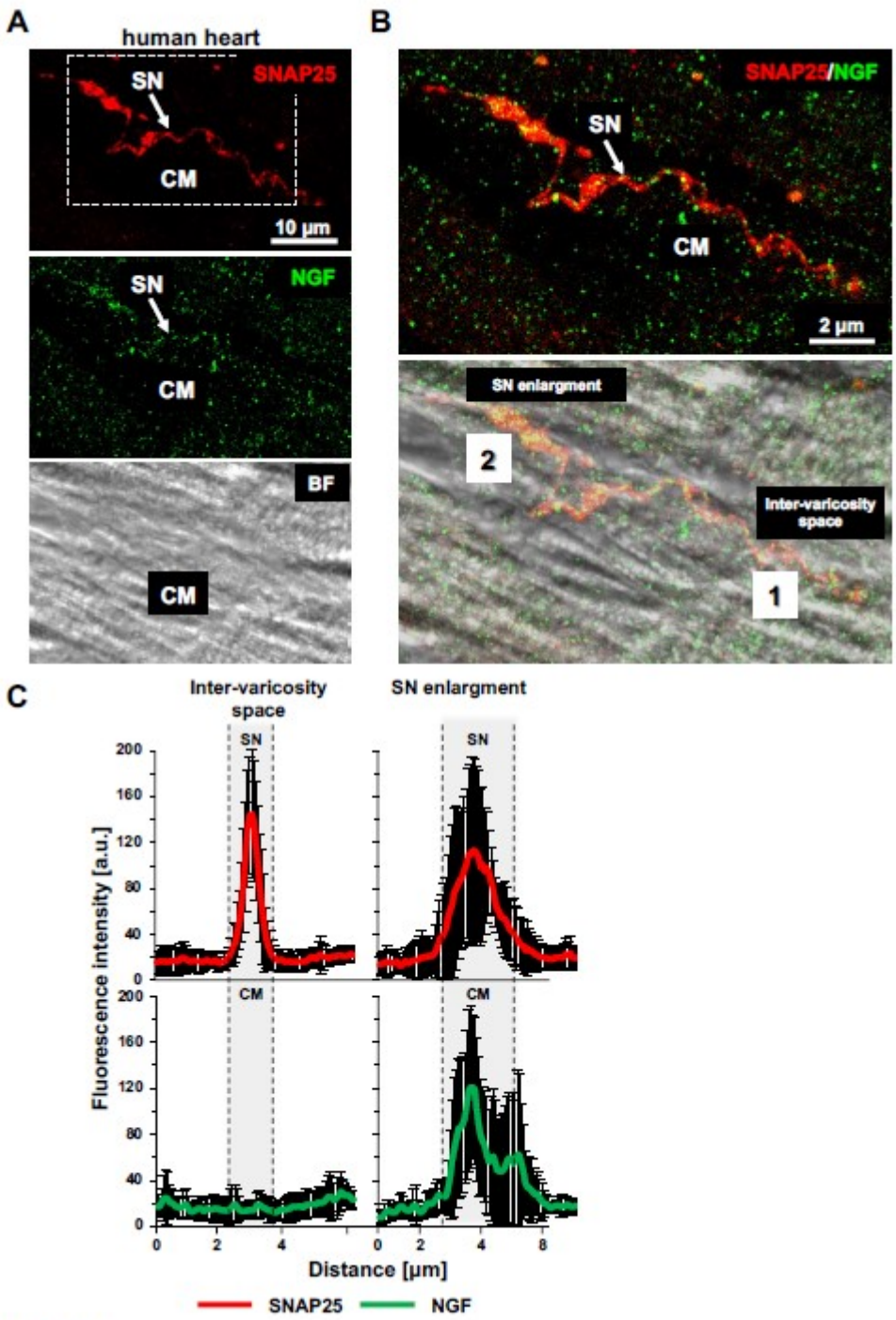

Figure 2

Figure 2. NGF mainly concentrates in the cardiomyocyte submembrane portion contacted by sympathetic neurons in human hearts.
(**A**) Confocal IF analysis of human heart sections, co-stained with antibodies against SNAP25 (top panel) and NGF (middle panel). The bottom panel shows the bright field image. (**B**) Magnification of the white box in (**A**), showing the merged fluorescence and bright field images. SN, sympathetic neurons; CM, cardiomyocyte. Arrows indicate NGF puncta in the neuronal process. (**C**) Quantification of the fluorescence intensity of SNAP25 (red signal) and NGF (green signal) in correspondence of the neuronal varicosity (2) or the inter-varicosity space (1). Bars represent SD (n=15 neuro-cardiac contacts from 2 different human hearts).

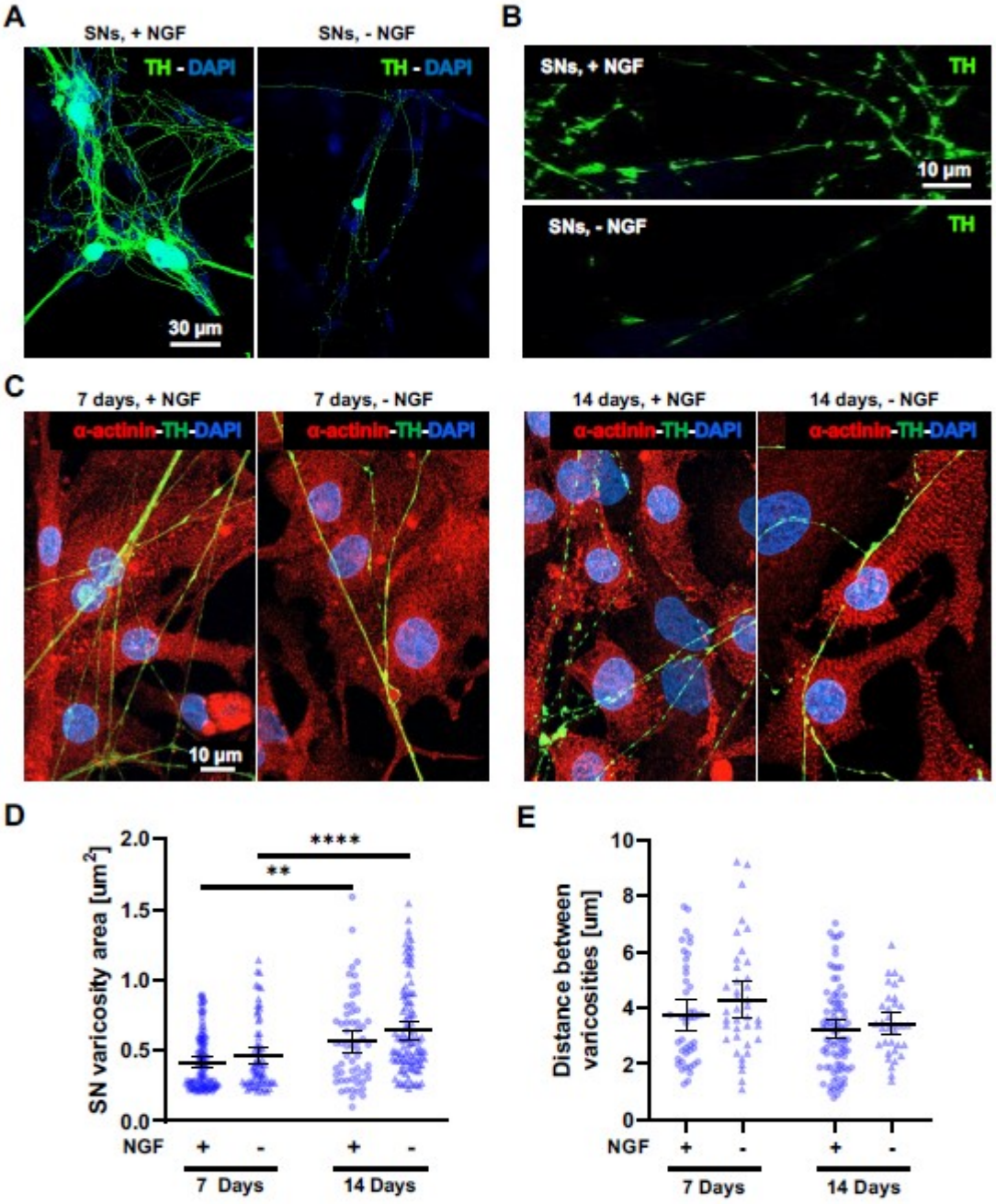

Figure 3

Figure 3. **Time- and neurotrophin-dependency of sympathetic neuron maturation in co-culture.**

(**A-B**) Confocal IF analysis of 7-days cSNs, isolated from the superior cervical and stellate ganglia of neonatal rats, cultured in the presence (+NGF) or the absence (-NGF) of NGF. Cells were stained with an antibody against tyrosine hydroxylase (TH). Nuclei were counterstained with DAPI. (**C**) Confocal IF analysis of 7 (left panels) *vs.* 14-days (right panels) SN/CM co-cultures, maintained in the presence or in

the absence of NGF. Cells were co-stained with antibodies agains α-actinin and TH. Nuclei were counterstained with DAPI. (**D-E**) Quantification of SN varicosity area (**D**) and interindividual distance between varicosities (**E**) in cSNs co-cultured with CMs, in the absence (-) *vs.* the presence (+) of NGF in the culture medium. Data distribution is represented by the individual values. Mean and error bars, representing 95% confidence interval, are shown. Differences among groups were determined using Mann-Whitney test. (**, $p<0.01$; ****, $p<0.0001$; (+) 7 Days n=101 and n=44; (+) 14 Days n=60 and n=85; (-) 7 days n=67 and n=39; (-) 14 days n=102 and n=34 varicosities for each group. Three independent cell preparations were analyzed).

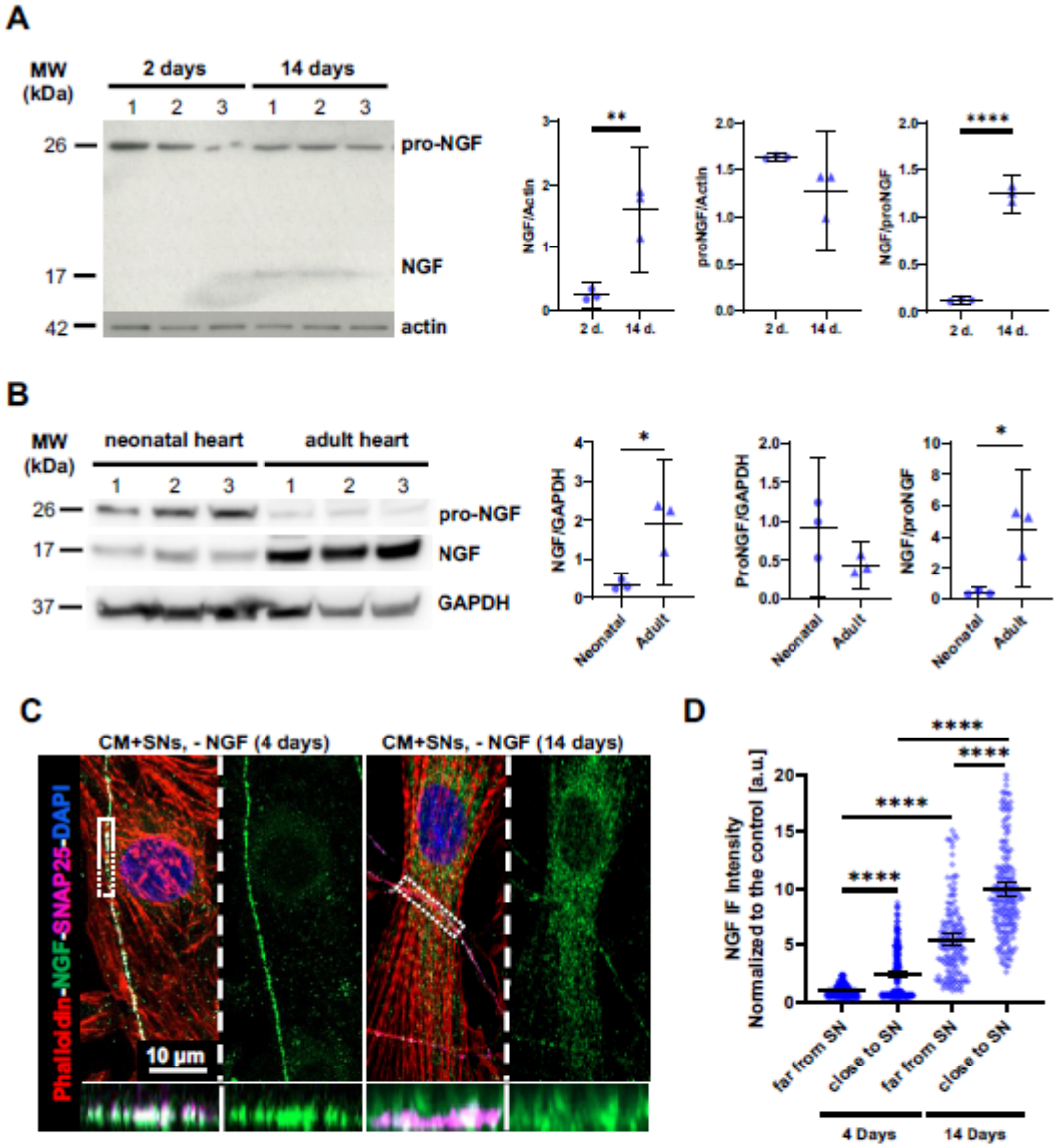

Figure 4

Figure 4. Time-dependency of NGF content and distribution in cardiomyocytes.

(A) Western blotting of pro-NGF and mature NGF (left panel) on protein extracts from CMs maintained for 2 or 14 days in culture. Actin was used as loading control. The right panels show the relative densitometry. Data distribution is represented by the individual values. Mean and error bars, representing 95% confidence interval, are shown. Differences among groups were determined using unpaired t-test or

Mann-Whitney test. (**, p<0.01; ****, p<0.0001. Three independent experiments were performed). **(B)** Western blotting of pro-NGF and mature NGF (left panel) on protein extracts from neonatal (P7) and adult (3 mo.) rat hearts. GAPDH was used as loading control. The right panel shows the relative densitometry. Data distribution is represented by the individual values. Mean and error bars, representing 95% confidence interval, are shown. Differences among groups were determined using unpaired t-test. (*, p<0.05; n=3 hearts for each group. Three independent experiments were performed). **(C)** Confocal IF analysis on 4 *vs.* 14-days SN/CM co-cultures maintained in the absence of exogenous NGF in the culture medium. Cells were co-stained with antibodies against NGF and SNAP25. CMs were stained with Alexa633-conjugated phalloidin, while nuclei were counterstained with DAPI. Bottom panels show resliced images of the boxed area highlighting the intercellular interface. **(D)** Comparison of the fluorescence intensity of NGF signal in CM portions close to- or far from the contacting innervating neuronal process, in the culture conditions described in **(C)**. Data distribution is represented by the individual values. Mean and error bars, representing 95% confidence interval, are shown. Differences among groups were determined using Mann-Whitney test. (****, p<0.0001; 4 Days: n=267 (far) and 296 (close); 14 Days: n=150 (far) and 192 (close) areas analyzed/group. Three independent cell preparations were analysed).

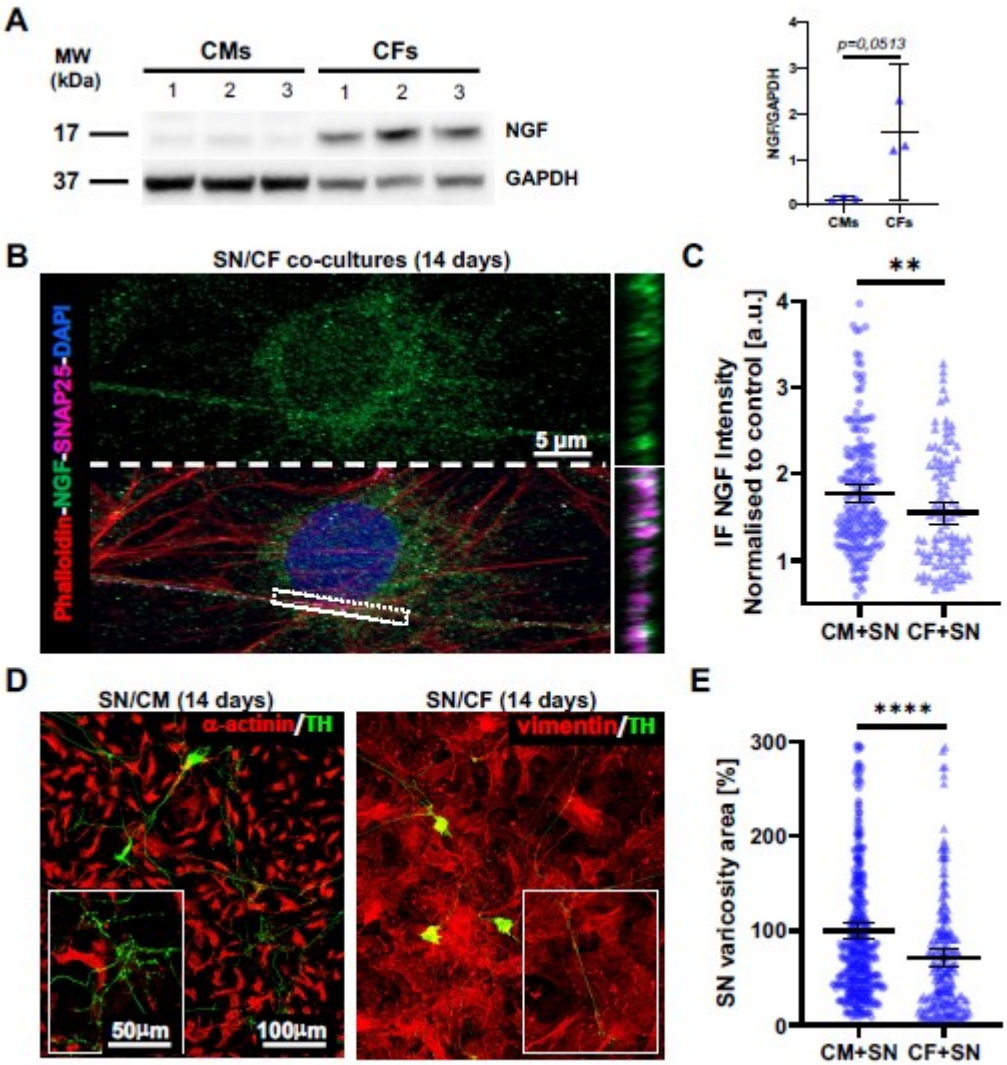

Figure 5

Figure 5. Sympathetic neurons co-cultured with cardiac fibroblasts require exogenous NGF.

(A) Western blotting of NGF protein content on extracts from CFs and CMs, maintained in culture for 14 days, in the absence of exogenous NGF. Actin was used to as loading control. The right panel shows the relative densitometry. Data distribution is represented by the individual values. Mean and error bars, representing 95% confidence interval, are shown. Differences among groups were determined using unpaired t-test. (Three independent experiments were performed). **(B)** Confocal IF analysis of 14-days SN/CF co-cultures maintained in the absence of exogenous NGF in the culture medium. Cells were co-stained with antibodies against SNAP25 and NGF and counterstained with Alexa633-conjugated phalloidin and DAPI. Bottom panels show resliced images of the boxed area highlighting the intercellular interface.

(C) Quantification of the mean NGF fluorescence intensity in the portion of SN processes contacting CMs (black bars) *vs.* CFs (grey bars). Data distribution is represented by the individual values. Mean and error bars, representing 95% confidence interval, are shown. Differences among groups were determined using Mann-Whitney test. (**, $p<0.01$; SN/CM: n=186 and SN/CF: n=104 areas analyzed/group. Three independent cell preparations were analyzed). **(D)** Confocal IF analysis of 14-days SN/CM (left panel) *vs.* SN/CF (right panel) co-cultures maintained in the absence of exogenous NGF. Cells were co-stained with antibodies against tyrosine hydroxylase (TH) and either anti-α-actinin (for SN/CM co-cultures) or anti-vimentin (for SN/CF co-cultures). **(E)** Quantification of the mean area of neuronal varicosities in contact with either CMs *or.* CFs. To highlight the differences between the two independent populations, values of the area of SN/CF contact sites were normalized to the average area size of varicosities in contact with CM. Mean and error bars, representing 95% confidence interval, are shown. Differences among groups were determined using Mann-Whitney test. (****, $p<0.0001$; n= 24 cell couples for each group. Three independent cell preparations were analyzed).

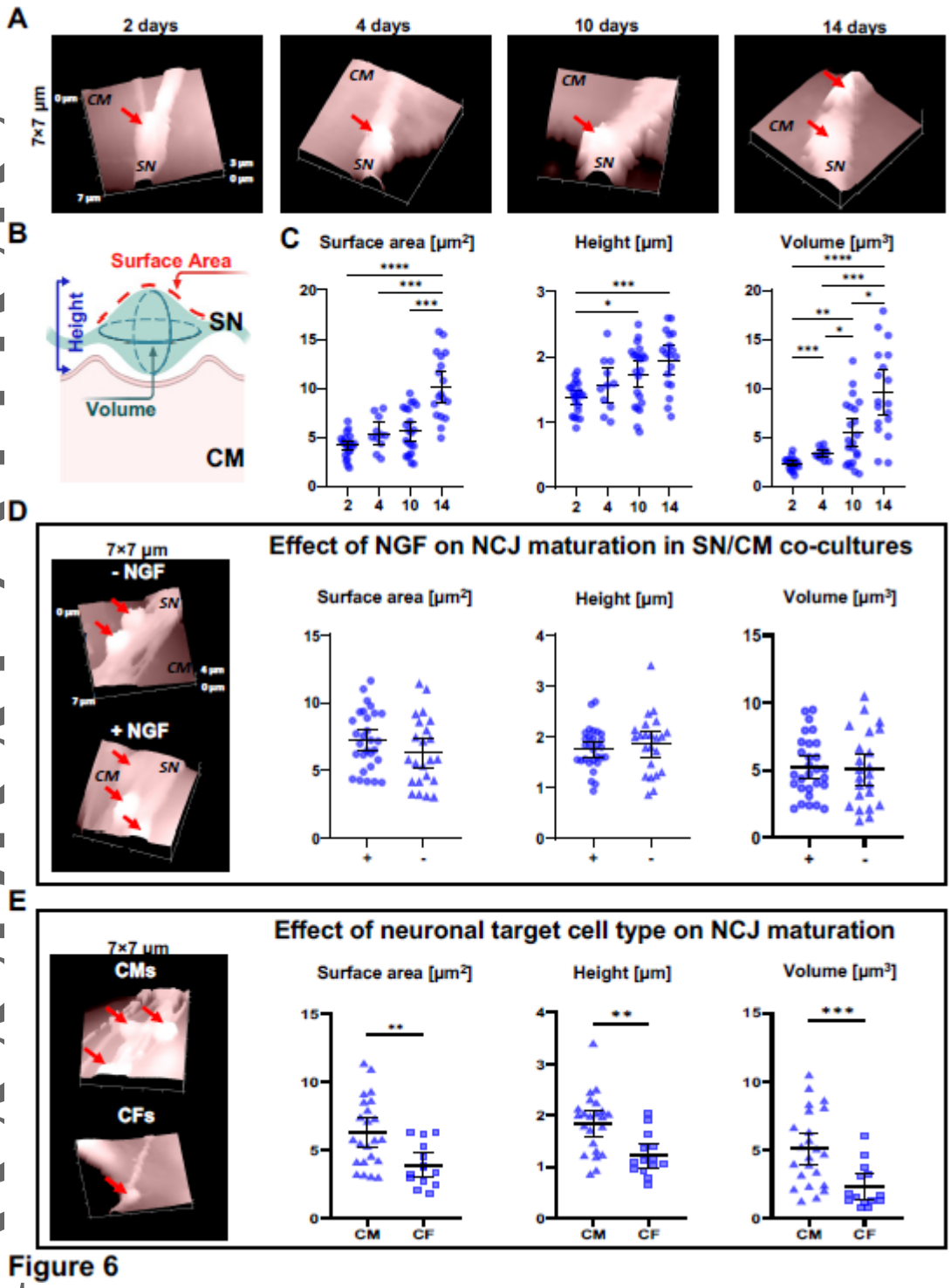

Figure 6

Figure 6. Surface topography of neuronal varicosities during co-culture maturation.

(A) Representative topographical images of SNs in 2-, 4-, 10- and 14-days co-culture with CM. Red arrows indicate neuronal varicosities. **(B)** Topographical parameters evaluated on SICM images and **(C)** relative measurements in SN/CM co-cultures analyzed at different time points. Data distribution is

represented by the individual values. Mean and error bars, representing 95% confidence interval, are shown. Differences among groups were determined using Brown-Forsythe test, with Dunnett's correction. (*, $p<0.05$; **, $p<0.01$; ***, $p<0.001$; ****, $p<0.0001$; n=15 SN/CM contacts for each group). **(D)** Representative SICM surface scans and quantification of relative parameters of the contact sites in 10-day SN-CM co-cultures, maintained in the absence (-) or the presence (+) of exogenous NGF. Data distribution is represented by the individual values. Mean and error bars, representing 95% confidence interval, are shown. Differences among groups were determined using unpaired t-test. (p=ns; n=23 SN/CM contacts for each group). **(E)** Representative SICM surface scans and quantification of relative parameters of the contact sites in 10-day SN/CF co-cultures, maintained in the absence of exogenous NGF. Data distribution is represented by the individual values. Mean and error bars, representing 95% confidence interval, are shown. Differences among groups were determined using unpaired t-test or Mann-Whitney test. (**, $p<0.01$; ***, $p<0.001$; SN/CM: n=23 and SN/CF: n=14 contacts).

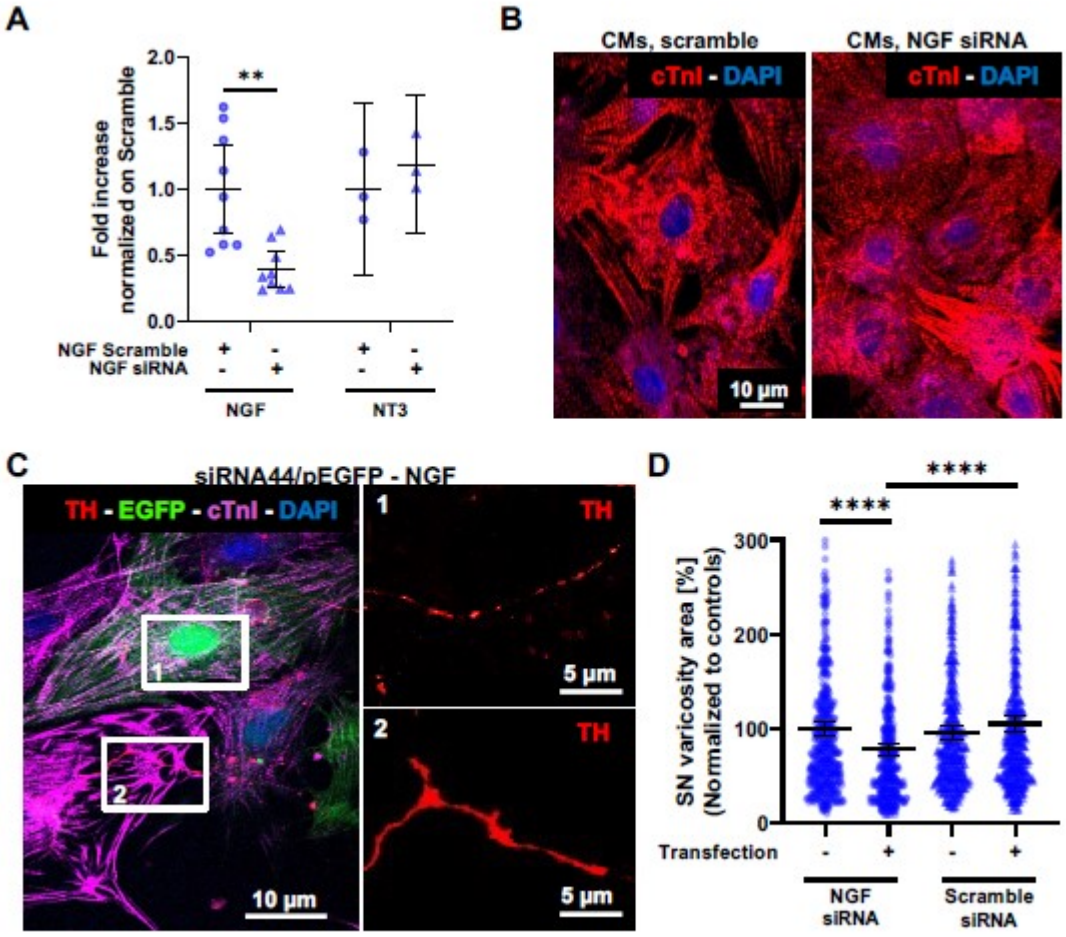

Figure 7

Figure 7. **Effect of NGF silencing in cardiomyocytes on co-cultured sympathetic neurons.**

(A) RTqPCR on extracts from cultured CMs transfected with scramble siRNA (white bars) or NGF siRNA (black bars). Data distribution is represented by the individual values. Mean and error bars, representing 95% confidence interval, are shown. Differences among groups were determined using unpaired t-test. (**, $p<0.01$; n=6 samples for each group in three independent cell preparations). **(B)** Confocal IF of cultured CMs transfected with either scramble siRNA or NGF siRNA. Cells were stained with an antibody against cardiac Troponin I (cTnI). Nuclei were counterstained with DAPI. **(C)** Confocal IF of 7-day SN/CM co-cultures in which CMs were co-transfected with GFP and NGF siRNA. Cells were co-stained with antibodies against tyrosine hydroxylase (TH) and cTnI. Nuclei were counterstained with DAPI. Images on the right are high magnifications of boxed areas on the left panel and show neuronal processes innervating respectively GFP+/NGF-silenced (1) or control (2) CMs. **(D)** Quantification of the mean area of TH+ sites contacting un-transfected, scramble-siRNA transfected or NGF-silenced CMs, in 7-day co-cultures maintained in the absence of exogenous NGF. Data distribution is represented by the individual values. Mean and error bars, representing 95% confidence interval, are shown. Differences among groups were determined using Mann-Whitney test. (****, $p<0.0001$; n>400 neuronal processes for each condition, in three independent cell preparations).

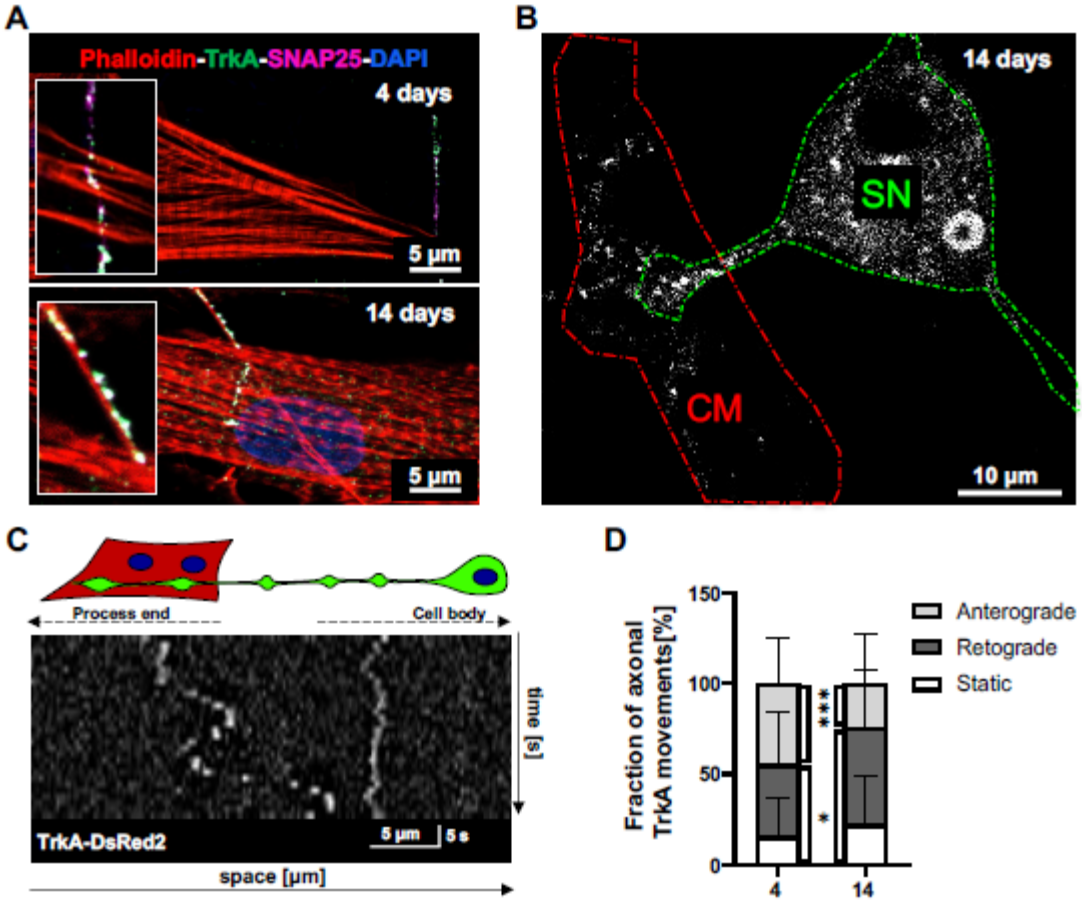

Figure 8

Figure 8. TrkA signaling assay in sympathetic neurons during time in co-culture.

(A) Confocal IF analysis of 4 (top panel) *vs.* 14 (bottom panel) day co-cultures co-stained with antibodies against TrkA and SNAP25. Cells were co-stained with Alexa633-conjugated phalloidin. Nuclei were counterstained with DAPI. **(B)** Confocal IF of SN/CM co-culture infected with an adenoviral vector encoding TrkA-DsRed2. The dashed lines indicate SN (green) and innervated CM (red). **(C)** Representative kymograph of TrkA-DsRed2 dots in one neuronal process of a 4-day SN/CM co-culture. **(D)** Quantification of TrkA-DsRed2 trafficking in SN processes contacting CMs, in early (4 days) and mature (14 days) co-cultures. Values are indicated as mean±SD. Differences among groups were determined using Mann-Whitney test. (*, $p<0.05$; ***, $p<0.001$; (4 days): n=47 and (14 days): n=40 cells per group. Three independent cell preparations were analyzed).

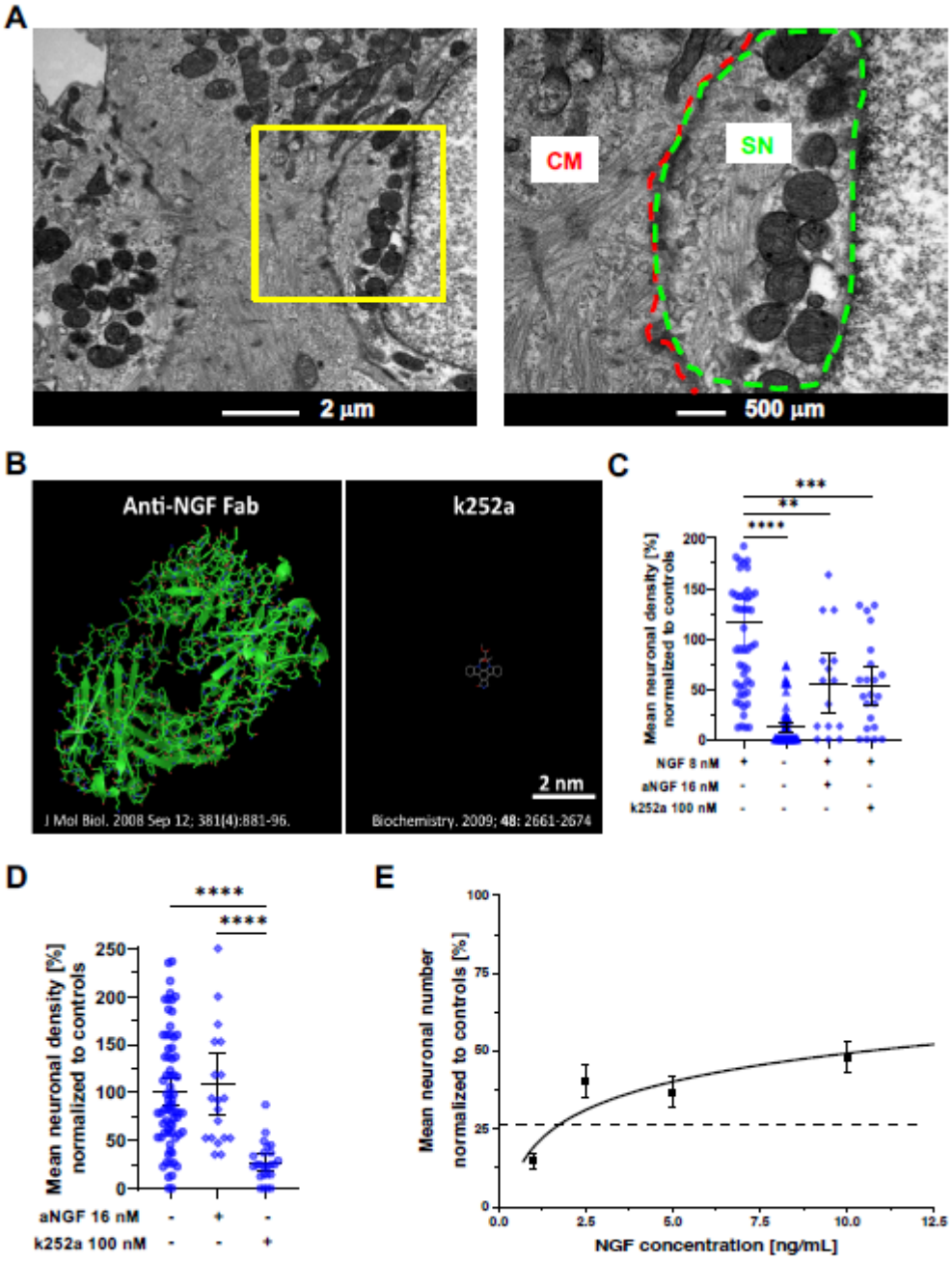

Figure 9

Figure 9. **Pharmacological assay of cardiomyocyte-neuron NGF signaling at the Neuro-Cardiac Junction.**

(A) Transmission electron microscopy of 14-day SN/CM co-cultures. The right panel is the magnification of the area in the left yellow inset. CM, cardiomyocyte; SN, sympathetic neuron. **(B)** Jmoll® 3D reconstruction of the Fab domain of an anti-NGF IgG and of k252a. **(C)** Quantification of the mean

neuronal density upon treatment of SN cultures with either anti-NGF or k252a. Data distribution is represented by the individual values. Mean and error bars, representing 95% confidence interval, are shown. Differences among groups were determined using Mann-Whitney test. (**, $p<0.01$; ***, $p<0.001$; ****, $p<0.0001$; n=35 fields/condition from 3 independent cell preparations). **(D)** Quantification of the mean neuronal density in SN/CM co-cultures treated as in **(C).** Data distribution is represented by the individual values. Mean and error bars, representing 95% confidence interval, are shown. Differences among groups were determined using Kruskal-Wallis test. (****, $p<0.0001$; n=35 fields/condition from 3 independent cell preparations). **(E)** Dose/effect curve of NGF on neuronal density in SN cultures treated with 100nM k252a. Interpolation was calculated using non-linear regression obtained with Microsoft Excel. Fitting line is shown (solid black). The dashed line indicates neuronal density in k252a treated SN/CM co-cultures. Bars indicate SD. (n=24 fields per conditions from 3 independent cell preparations).

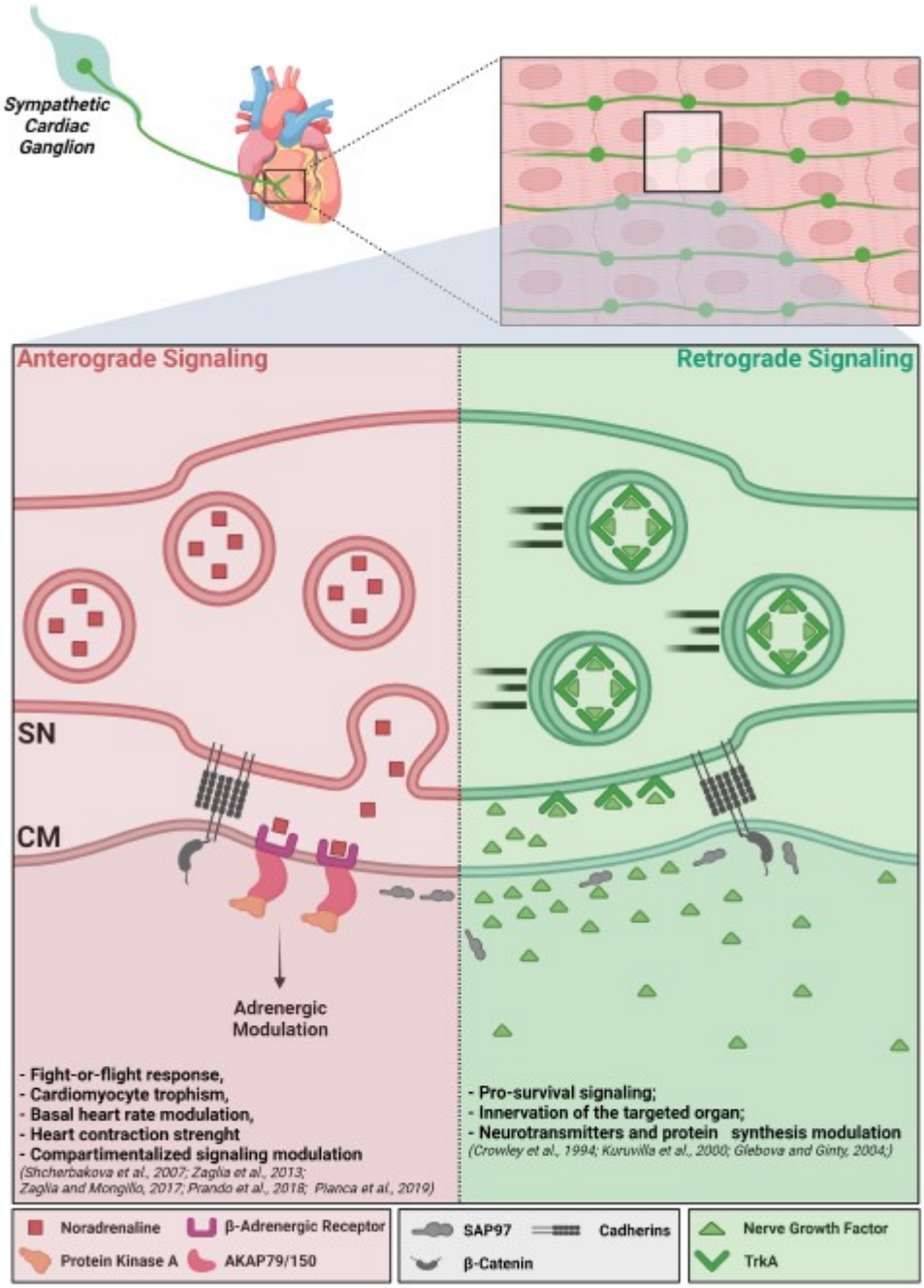

Figure 10. The Neuro-Cardiac Junction represents the functional unit underlying both anterograde and retrograde sympathetic neuron-cardiomyocyte communication.

(A) Roadmap of post-ganglionic SNs, from the cervical ganglia to the myocardial interstitium. **(B)** Cartoon representation of the NCJ is the election site of bi-directional SN-CM communication (created with BioRender.com).

REFERENCES

Berg MM, Sternberg DW, Parada LF & Chao M V (1992). K-252a inhibits nerve growth factor-induced trk proto-oncogene tyrosine phosphorylation and kinase activity. *J Biol Chem* **267,** 13–16.

Di Bona A, Vita V, Costantini I & Zaglia T (2020). Towards a clearer view of sympathetic innervation of cardiac and skeletal muscles. *Prog Biophys Mol Biol* **154,** 80–93. Available at: https://pubmed.ncbi.nlm.nih.gov/31337503/ [Accessed May 24, 2021].

Boogers MJ, Borleffs CJW, Henneman MM, van Bommel RJ, van Ramshorst J, Boersma E, Dibbets-Schneider P, Stokkel MP, van der Wall EE, Schalij MJ & Bax JJ (2010). Cardiac Sympathetic Denervation Assessed With 123-Iodine Metaiodobenzylguanidine Imaging Predicts Ventricular Arrhythmias in Implantable Cardioverter-Defibrillator Patients. *J Am Coll Cardiol* **55,** 2769–2777.

Cao J-M, Chen LS, KenKnight BH, Ohara T, Lee M-H, Tsai J, Lai WW, Karagueuzian HS, Wolf PL, Fishbein MC & Chen P-S (2000*a*). Nerve Sprouting and Sudden Cardiac Death. *Circ Res* **86,** 816–821.

Cao J-M, Fishbein MC, Han JB, Lai WW, Lai AC, Wu T-J, Czer L, Wolf PL, Denton TA, Shintaku IP, Chen P-S & Chen LS (2000*b*). Relationship Between Regional Cardiac Hyperinnervation and Ventricular Arrhythmia. *Circulation* **101,** 1960–1969.

Chao M V (2003). Neurotrophins and their receptors: A convergence point for many signaling pathways. *Nat Rev Neurosci* **4,** 299–309.

Colangelo AM, Johnson PF & Mocchetti I (1998). β-Adrenergic receptor-induced activation of nerve growth factor gene transcription in rat cerebral cortex involves CCAAT/enhancer-binding protein δ. *Proc Natl Acad Sci* **95,** 10920 LP – 10925.

Franzoso M, Zaglia T & Mongillo M (2016). Putting together the clues of the everlasting neuro-cardiac liaison. *Biochim Biophys Acta - Mol Cell Res* **1863,** 1904–1915.

Furukawa S, Furukawa Y, Satoyoshi E & Hayashi K (1987). Regulation of nerve growth factor synthesis/secretion by catecholamine in cultured mouse astroglial cells. *Biochem Biophys Res*

Commun **147,** 1048–1054.

Furukawa Y, Furukawa S, Satoyoshi E & Hayashi K (1986). Catecholamines induce an increase in nerve growth factor content in the medium of mouse L-M cells. *J Biol Chem* **261,** 6039–6047.

Furukawa Y, Tomioka N, Sato W, Satoyoshi E, Hayashi K & Furukawa S (1989). Catecholamines increase nerve growth factor mRNA content in both mouse astroglial cells and fibroblast cells. *FEBS Lett* **247,** 463–467.

Gardner RT, Ripplinger CM, Myles RC & Habecker BA (2016). Molecular Mechanisms of Sympathetic Remodeling and Arrhythmias. *Circ Arrhythmia Electrophysiol* **9,** e001359.

Glebova NO & Ginty DD (2004). Heterogeneous Requirement of NGF for Sympathetic Target Innervation In Vivo. *J Neurosci* **24,** 743–751.

Greene LA (1977). Quantitative in vitro studies on the nerve growth factor (NGF) requirement of neurons: I. Sympathetic neurons. *Dev Biol* **58,** 96–105.

Grundy D (2015). Principles and standards for reporting animal experiments in The Journal of Physiology and Experimental Physiology. *J Physiol* **593,** 2547–2549.

Habecker BA, Anderson ME, Birren SJ, Fukuda K, Herring N, Hoover DB, Kanazawa H, Paterson DJ & Ripplinger CM (2016). Molecular and cellular neurocardiology: development, and cellular and molecular adaptations to heart disease. *J Physiol* **594,** 3853–3875.

Habecker BA, Bilimoria P, Linick C, Gritman K, Lorentz CU, Woodward W & Birren SJ (2008). Regulation of cardiac innervation and function via the p75 neurotrophin receptor. *Auton Neurosci* **140,** 40–48.

Hanaoka Y, Ohi T, Furukawa S, Furukawa Y, Hayashi K & Matsukura S (1994). The therapeutic effects of 4-methylcatechol, a stimulator of endogenous nerve growth factor synthesis, on experimental diabetic neuropathy in rats. *J Neurol Sci* **122,** 28–32.

Hansma PK, Drake B, Marti O, Gould SAC & Prater CB (1989). The scanning ion-conductance microscope. *Science (80-)* **243,** 641–643.

Hasan W, Jama A, Donohue T, Wernli G, Onyszchuk G, Al-Hafez B, Bilgen M & Smith PG (2006).

Sympathetic hyperinnervation and inflammatory cell NGF synthesis following myocardial infarction in rats. *Brain Res* **1124,** 142–154.

Herring N, Kalla M, Paterson DJ (2019).The autonomic nervous system and cardiac arrhythmias: current concepts and emerging therapies. *Nat Rev Cardiol* **16(12)**, 707-726.

Heumann R, Korsching S, Scott J & Thoenen H (1984). Relationship between levels of nerve growth factor (NGF) and its messenger RNA in sympathetic ganglia and peripheral target tissues. *EMBO J* **3,** 3183–3189.

Himura Y, Felten SY, Kashiki M, Lewandowski TJ, Delehanty JM & Liang CS (1993). Cardiac noradrenergic nerve terminal abnormalities in dogs with experimental congestive heart failure. *Circulation* **88,** 1299–1309.

Ieda M, Fukuda K, Hisaka Y, Kimura K, Kawaguchi H, Fujita J, Shimoda K, Takeshita E, Okano H, Kurihara Y, Kurihara H, Ishida J, Fukamizu A, Federoff HJ & Ogawa S (2004). Endothelin-1 regulates cardiac sympathetic innervation in the rodent heart by controlling nerve growth factor expression. *J Clin Invest* **113,** 876–884.

Ieda M, Kanazawa H, Kimura K, Hattori F, Ieda Y, Taniguchi M, Lee J-K, Matsumura K, Tomita Y, Miyoshi S, Shimoda K, Makino S, Sano M, Kodama I, Ogawa S & Fukuda K (2007). Sema3a maintains normal heart rhythm through sympathetic innervation patterning. *Nat Med* **13,** 604–612.

Jakobs MA, Dimitracopoulos A & Franze K (2019). Kymobutler, a deep learning software for automated kymograph analysis. *Elife*; DOI: 10.7554/ELIFE.42288.

Kaechi K, Furukawa Y, Ikegami R, Nakamura N, Omae F, Hashimoto Y, Hayashi K & Furukawa S (1993). Pharmacological induction of physiologically active nerve growth factor in rat peripheral nervous system. *J Pharmacol Exp Ther* **264,** 321 LP – 326.

Kawano H, Okada R & Yano K (2003). Histological study on the distribution of autonomic nerves in the human heart. *Heart Vessels* **18,** 32–39.

Kaye DM, Vaddadi G, Gruskin SL, Du X-J & Esler MD (2000). Reduced Myocardial Nerve Growth

Factor Expression in Human and Experimental Heart Failure. *Circ Res* **86,** e80–e84.

Kimura K, Ieda M & Fukuda K (2012). Development, Maturation, and Transdifferentiation of Cardiac Sympathetic Nerves. *Circ Res* **110,** 325–336.

Kimura K, Ieda M, Kanazawa H, Yagi T, Tsunoda M, Ninomiya SI, Kurosawa H, Yoshimi K, Mochizuki H, Yamazaki K, Ogawa S & Fukuda K (2007). Cardiac sympathetic rejuvenation: A link between nerve function and cardiac hypertrophy. *Circ Res* **100,** 1755–1764.

Kimura K, Kanazawa H, Ieda M, Kawaguchi-Manabe H, Miyake Y, Yagi T, Arai T, Sano M & Fukuda K (2010). Norepinephrine-induced nerve growth factor depletion causes cardiac sympathetic denervation in severe heart failure. *Auton Neurosci Basic Clin* **156,** 27–35.

Kiriazis H, Jennings NL, Davern P, Lambert G, Su Y, Pang T, Du X, La Greca L, Head GA, Hannan AJ & Du X-J (2012). Neurocardiac dysregulation and neurogenic arrhythmias in a transgenic mouse model of Huntington's disease. *J Physiol* **590,** 5845–5860.

Kobal J, Meglič B, Mesec A & Peterlin B (2004). Early sympathetic hyperactivity in Huntington's disease. *Eur J Neurol* **11,** 842–848.

Kuruvilla R, Ye H & Ginty DD (2000). Spatially and Functionally Distinct Roles of the PI3-K Effector Pathway during NGF Signaling in Sympathetic Neurons. *Neuron* **27,** 499–512.

Larsen HE, Lefkimmiatis K & Paterson DJ (2016). Sympathetic neurons are a powerful driver of myocyte function in cardiovascular disease. *Sci Rep*; DOI: 10.1038/srep38898.

Li S-T, Tack CJ, Fananapazir L & Goldstein DS (2000). Myocardial perfusion and sympathetic innervation in patients with hypertrophic cardiomyopathy. *J Am Coll Cardiol* **35,** 1867–1873.

Lockhart ST, Turrigiano GG & Birren SJ (1997). Nerve Growth Factor Modulates Synaptic Transmission between Sympathetic Neurons and Cardiac Myocytes. *J Neurosci* **17,** 9573 LP – 9582.

Lorentz CU, Alston EN, Belcik T, Lindner JR, Giraud GD & Habecker BA (2010). Heterogeneous ventricular sympathetic innervation, altered β-adrenergic receptor expression, and rhythm instability in mice lacking the p75 neurotrophin receptor. *Am J Physiol Circ Physiol* **298,** H1652–

H1660.

Mains RE & Patterson PH (1973). PRIMARY CULTURES OF DISSOCIATED SYMPATHETIC NEURONS : I. Establishment of Long-Term Growth in Culture and Studies of Differentiated Properties . *J Cell Biol* **59,** 329–345.

Mias C, Coatrieux C, Denis C, Genet G, Seguelas M-H, Laplace N, Rouzaud-Laborde C, Calise D, Parini A, Cussac D, Pathak A, Sénard J-M & Galés C (2013). Cardiac Fibroblasts Regulate Sympathetic Nerve Sprouting and Neurocardiac Synapse Stability. *PLoS One* **8,** e79068.

Miyauchi Y, Zhou S, Okuyama Y, Miyauchi M, Hayashi H, Hamabe A, Fishbein MC, Mandel WJ, Chen LS, Chen P-S & Karagueuzian HS (2003). Altered Atrial Electrical Restitution and Heterogeneous Sympathetic Hyperinnervation in Hearts With Chronic Left Ventricular Myocardial Infarction. *Circulation* **108,** 360–366.

Nishisato K, Hashimoto A, Nakata T, Doi T, Yamamoto H, Nagahara D, Shimoshige S, Yuda S, Tsuchihashi K & Shimamoto K (2010). Impaired Cardiac Sympathetic Innervation and Myocardial Perfusion Are Related to Lethal Arrhythmia: Quantification of Cardiac Tracers in Patients with ICDs. *J Nucl Med* **51,** 1241 LP – 1249.

Novak P, Li C, Shevchuk AI, Stepanyan R, Caldwell M, Hughes S, Smart TG, Gorelik J, Ostanin VP, Lab MJ, Moss GWJ, Frolenkov GI, Klenerman D & Korchev YE (2009). Nanoscale live-cell imaging using hopping probe ion conductance microscopy. *Nat Methods* **6,** 279–281.

Orimo S, Takahashi A, Uchihara T, Mori F, Kakita A, Wakabayashi K & Takahashi H (2007). Degeneration of Cardiac Sympathetic Nerve Begins in the Early Disease Process of Parkinson's Disease. *Brain Pathol* **17,** 24–30.

Pianca N, Di Bona A, Lazzeri E, Costantini I, Franzoso M, Prando V, Armani A, Rizzo S, Fedrigo M, Angelini A, Basso C, Pavone FS, Rubart M, Sacconi L, Zaglia T & Mongillo M (2019). Cardiac sympathetic innervation network shapes the myocardium by locally controlling cardiomyocyte size through the cellular proteolytic machinery. *J Physiol* **597,** 3639–3656.

Prando V, Da Broi F, Franzoso M, Plazzo AP, Pianca N, Francolini M, Basso C, Kay MW, Zaglia T & Mongillo M (2018). Dynamics of neuroeffector coupling at cardiac sympathetic synapses. *J*

Physiol **596,** 2055–2075.

Reichardt LF (2006). Neurotrophin-regulated signaling pathways. *Philos Trans R Soc B Biol Sci* **361,** 1545–1564.

Scalco A, Moro N, Mongillo M & Zaglia T (2021). Neurohumoral Cardiac Regulation: Optogenetics Gets Into the Groove. *Front Physiol* **12,** 1323. Available at: https://www.frontiersin.org/article/10.3389/fphys.2021.726895.

Schäfers M, Dutka D, Rhodes CG, Lammertsma AA, Hermansen F, Schober O & Camici PG (1998). Myocardial Presynaptic and Postsynaptic Autonomic Dysfunction in Hypertrophic Cardiomyopathy. *Circ Res* **82,** 57–62.

Saggin L, Gorza L, Ausoni S, Schiaffino S (1989). Troponin I switching in the developing heart. *J Biol Chem.* **264**(27), 16299-302.

Shan J, Kushnir A, Betzenhauser MJ, Reiken S, Li J, Lehnart SE, Lindegger N, Mongillo M, Mohler PJ & Marks AR (2010). Phosphorylation of the ryanodine receptor mediates the cardiac fight or flight response in mice. *J Clin Invest* **120,** 4388–4398.

Shcherbakova OG, Hurt CM, Xiang Y, Dell'Acqua ML, Zhang Q, Tsien RW & Kobilka BK (2007). Organization of β-adrenoceptor signaling compartments by sympathetic innervation of cardiac myocytes. *J Cell Biol* **176,** 521–533.

Shelton DL & Reichardt LF (1984). Expression of the beta-nerve growth factor gene correlates with the density of sympathetic innervation in effector organs. *Proc Natl Acad Sci* **81,** 7951 LP – 7955.

Tapa S, Wang L, Francis Stuart SD, Wang Z, Jiang Y, Habecker BA & Ripplinger CM (2020). Adrenergic supersensitivity and impaired neural control of cardiac electrophysiology following regional cardiac sympathetic nerve loss. *Sci Rep* **10,** 18801.

Terai H, Shimizu M, Ino H, Yamaguchi M, Uchiyama K, Oe K, Nakajima K, Taki J, Kawano M & Mabuchi H (2003). Changes in Cardiac Sympathetic Nerve Innervation and Activity in Pathophysiologic Transition from Typical to End-Stage Hypertrophic Cardiomyopathy. *J Nucl*

Med **44,** 1612 LP – 1617.

Wichter T, Matheja P, Eckardt L, Kies P, Schäfers K, Schulze-Bahr E, Haverkamp W, Borggrefe M, Schober O, Breithardt G & Schäfers M (2002). Cardiac Autonomic Dysfunction in Brugada Syndrome. *Circulation* **105,** 702–706.

Zaglia T, Di Bona A, Chioato T, Basso C, Ausoni S & Mongillo M (2016). Optimized protocol for immunostaining of experimental GFP-expressing and human hearts. *Histochem Cell Biol* **146,** 407–419.

Zaglia T, Milan G, Franzoso M, Bertaggia E, Pianca N, Piasentini E, Voltarelli VA, Chiavegato D, Brum PC, Glass DJ, Schiaffino S, Sandri M & Mongillo M (2013). Cardiac sympathetic neurons provide trophic signal to the heart via β2-adrenoceptor-dependent regulation of proteolysis. *Cardiovasc Res* **97,** 240–250.

Zaglia T, Milan G, Ruhs A, Franzoso M, Bertaggia E, Pianca N, Carpi A, Carullo P, Pesce P, Sacerdoti D, Sarais C, Catalucci D, Krüger M, Mongillo M & Sandri M (2014). Atrogin-1 deficiency promotes cardiomyopathy and premature death via impaired autophagy. *J Clin Invest* **124,** 2410–2424.

Zaglia T & Mongillo M (2017). Cardiac sympathetic innervation, from a different point of (re)view. *J Physiol* **595,** 3919–3930.

Zhou S, Chen LS, Miyauchi Y, Miyauchi M, Kar S, Kangavari S, Fishbein MC, Sharifi B & Chen P-S (2004). Mechanisms of Cardiac Nerve Sprouting After Myocardial Infarction in Dogs. *Circ Res* **95,** 76–83.

Zweifel LS, Kuruvilla R & Ginty DD (2005). Functions and mechanisms of retrograde neurotrophin signaling. *Nat Rev Neurosci* **6,** 615–625.

AUTHORS' PROFILE

Lolita Dokshokova, MSc, PhD, is a physicist, who recently completed her PhD in Cardiovascular Sciences, at the University of Verona. Lolita spent part of his PhD in Padova, in the Zaglia and Mongillo laboratories, and part in London, in Gorelik's lab. The synergy of skills in physics, with those acquired in biology, allowed Lolita to implement *in vitro* co-culture systems and study intercellular signaling with advanced microscopy techniques.

Mauro Franzoso, MSc, PhD is a biotechnologist, who received his PhD in Biomedical Sciences, at the University of Padova. Mauro dedicated himself to *in vitro* and *ex vivo* studies aimed at dissecting the mechanisms regulating heart sympathetic innervation, with a focus on the retrograde, neurotrophin-mediated, 'cardiomyocyte-to-sympathetic neuron' communication, in physiology and pathology.

The research pursued by Drs. Dokshokova and Franzoso has recently been awarded *best poster presentation* at the European section of the International Society for Heart Research Congress (ISHR 2021), held in Turin.

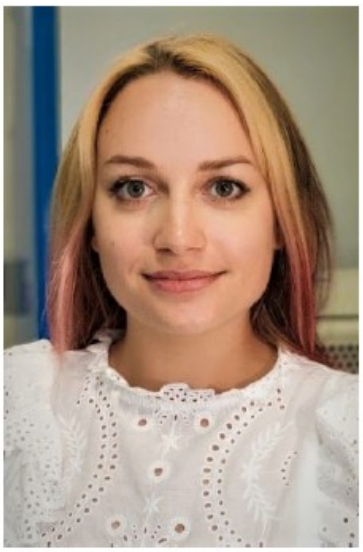

Lolita Dokshokova
MSc, PhD

Mauro Franzoso
MSc, PhD

Target	Company	Host	Dilution
α-actinin	Sigma-Aldrich	mouse	1:200
cardiac Troponin I	(Saggin *et al.*, 1989)	mouse	1:200
Nerve Growth Factor	Abcam	rabbit	1:100
SNAP25	Abcam	mouse	1:200
Tyrosine Hydroxylase	Millipore	rabbit	1:400
Tyrosine Hydroxylase	Millipore	sheep	1:100
TrkA	Alomone	rabbit	1:200
vimentin	Sigma-Aldrich	mouse	1:200

Table 1. Primary antibodies used in this study.

Antibody	Company	Host	Dilution
Anti-mouse Alexa Fluor-647	Invitrogen	rabbit	1:300
Anti-mouse Cy3	Jackson	goat	1:200
Anti-rabbit Alexa Fluor 488	Jackson	goat	1:200
Anti-rabbit Alexa Fluor 647	Jackson	donkey	1:200
Anti-rabbit Cy3	Jackson	goat	1:200
Anti-sheep TRITC	Jackson	donkey	1:100

Table 2. Secondary antibodies used in this study.

Name	Company	Dilution
Alexa Fluor 633-phalloidin	Invitrogen	1:200
DAPI	Invitrogen	1:5000

Table 3. Chemicals used in IF experiments.

Primer name	Sequence
Rat NGF Forward	5'-TGACAGTGCTGGGCGAGGTGAA-3'
Rat NGF Reverse	5'-TCAATGCCCCGGCATCCACTCT-3'
Rat NT3 Forward	5'-CATAAGAGTCACCGAGGAGAGTACT-3'
Rat NT3 Forward	5'-ATGTCAATGGCTGAGGACTTGTC-3'
Rat GAPDH Forward	5'-AGGGCTGCCTTCTCTTGTGAC-3'
Rat GAPDH Reverse	5'-TGGGTACAGTCATACTGGAACATGTAG-3'
Rat β actin Forward	5'-CTGGCTCCTAGCACCATGAAGAT-3'
Rat β actin Reverse	5'-GGTGGACAGTGAGGCCAGGAT-3'

Table 4: Oligoes used in RTqPCR experiments.